



**HAL**  
open science

# Modelling of a Phase Change Material Melting Process Heated from below Using Spectral Collocation Methods

Jean Batina, Serge Blancher, Tarik Kousksou

► **To cite this version:**

Jean Batina, Serge Blancher, Tarik Kousksou. Modelling of a Phase Change Material Melting Process Heated from below Using Spectral Collocation Methods. *International Journal of Numerical Methods for Heat and Fluid Flow*, 2014, 24 (3), pp.697-734. 10.1108/HFF-03-2012-0062 . hal-02153542

**HAL Id: hal-02153542**

**<https://univ-pau.hal.science/hal-02153542>**

Submitted on 27 Apr 2024

**HAL** is a multi-disciplinary open access archive for the deposit and dissemination of scientific research documents, whether they are published or not. The documents may come from teaching and research institutions in France or abroad, or from public or private research centers.

L'archive ouverte pluridisciplinaire **HAL**, est destinée au dépôt et à la diffusion de documents scientifiques de niveau recherche, publiés ou non, émanant des établissements d'enseignement et de recherche français ou étrangers, des laboratoires publics ou privés.

# Modelling of a Phase Change Material melting process heated from below using spectral collocation methods

Jean Batina, Serge Blancher and Tarik Kouskou  
Génie Thermique et Energie, IUT des Pays de l'Adour,  
Pau, France

**Purpose** – Mathematical and numerical models are developed to study the melting of a Phase Change Material (PCM) inside a 2D cavity. The bottom of the cell is heated at constant and uniform temperature or heat flux, assuming that the rest of the cavity is completely adiabatic. The paper used suitable numerical methods to follow the interface temporal evolution with a good accuracy. The purpose of this paper is to show how the evolution of the latent energy absorbed to melt the PCM depends on the temperature imposed on the lower wall of the cavity.

**Design/methodology/approach** – The problem is written with non-homogeneous boundary conditions. Momentum and energy equations are numerically solved in space by a spectral collocation method especially oriented to this situation. A Crank-Nicolson scheme permits the resolution in time.

**Findings** – The results clearly show the evolution of multicellular regime during the process of fusion and the kinetics of phase change depends on the boundary condition imposed on the bottom cell wall. Thus the charge and discharge processes in energy storage cells can be controlled by varying the temperature in the cell PCM. Substantial modifications of the thermal convective heat and mass transfer are highlighted during the transient regime. This model is particularly suitable to follow with a good accuracy the evolution of the solid/liquid interface in the process of storage/release energy.

**Research limitations/implications** – The time-dependent physical properties that induce non-linear coupled unsteady terms in Navier-Stokes and energy equations are not taken into account in the present model. The present model is actually extended to these coupled situations. This problem requires smoother geometries. One can try to palliate this disadvantage by constructing smoother approximations of non-smooth geometries. The augmentation of polynomials developments orders increases strongly the computing time. When the external heat flux or temperature imposed at the PCM is much greater than the temperature of the PCM fusion, one must choose carefully some data to assume the algorithms convergence.

**Practical implications** – Among the areas where this work can be used, are: buildings where the PCM are used in insulation and passive cooling; thermal energy storage, the PCM stores energy by changing phase, solid to liquid (fusion); cooling and transport of foodstuffs or pharmaceutical or medical sensitive products, the PCM is used in the food industry, pharmaceutical and medical, to minimize temperature variations of food, drug or sensitive materials; and the textile industry, PCM materials in the textile industry are used in microcapsules placed inside textile fibres. The PCM intervene to regulate heat transfer between the body and the outside.

**Originality/value** – The paper's originality is reflected in the precision of its results, due to the use of a high-accuracy numerical approximation based on collocation spectral methods, and the choice of Chebyshev polynomials basis in both axial and radial directions.

**Keywords** Phase Change Material, Charge and discharge processes, Energy storage cells, Convective heat transfer, Spectral collocation methods, High-accuracy numerical approximation, Crank-Nicolson resolution in time

## Nomenclature

$a$	thermal diffusivity ( $a = \lambda/(\rho C_p)$ ) ( $\text{m}^2/\text{s}^{-1}$ )	<i>Greek symbols</i>
$c_p$	thermal capacity ( $\text{J}/(\text{kg K})$ )	$\beta$
$g$	acceleration of gravity ( $\text{m}/\text{s}^2$ )	
$h$	liquid layer half thickness, $h = (H_T - H_L)/2$ (m)	$\Phi_W$
$H_I$	height of the solid-liquid interface (m)	$\theta$
$H_L$	height of the cell bottom wall (m)	$\lambda$
$H_S$	height of the cell top wall (m)	$\mu$
$L$	half-length of the PCM cell (m)	$\nu$
$La$	latent heat ( $\text{J}/\text{kg}$ )	$\nu = \mu/\rho$ ( $\text{m}^2/\text{s}$ )
$Nu$	Nusselt number	$\rho$
$Pr$	Prandtl number	$\omega$
$Ra$	Rayleigh number	$\psi$
$Ste$	Stephan number	
$T$	Chebyshev polynomial	<i>Subscripts</i>
$t$	time (s)	$M$
$\vec{V}$	$= (u, v)$ velocity field	$I$
$u$	$z$ component of velocity ( $\text{m}/\text{s}$ )	$L$
$v$	$y$ component of velocity ( $\text{m}/\text{s}$ )	$S$
$y$	vertical coordinate (m)	$W$
$z$	horizontal coordinate (m)	$top$
		$O$

## 1. Introduction

Currently, the protection of the environment and the energy consumption savings are critical and inescapable areas of economic development. Smart materials, real technological innovations, appeared on the market to solve this both ecological and economic dual challenge: the Phase Change Materials (PCMs). Among the areas where they are most used, we can mention:

- The building, where the PCM are used in insulation and passive cooling. Because of global warming, energy consumption for air conditioning is increasing, impacting highly the environment. PCMs have a definite advantage to reduce cooling needs of buildings: placed in walls, they melt and absorb excess heat when the outside temperature exceeds the PCM melting temperature (at day for example) and they solidify, restoring the stored energy, when the temperature decreases (at night for example).
- Thermal energy storage. The PCM stores energy by changing phase, solid to liquid (melting). Then they restore heat by the phase change liquid to solid (freezing). One can, for example, store the heat removed by a garbage incinerator in PCM containers. The energy release is then recovered on suitable workstations.
- Cooling and transport of foodstuffs or pharmaceutical or medical sensitive products. The PCM is used in the food industry, pharmaceutical and medical, to minimize temperature variations of food, drug or sensitive materials such as in the case of blood transportation. They occur mostly in the form of small plastic “bags” containing suitable PCM, which are positioned closer to the product to be preserved.
- The textile industry. PCM materials in the textile industry are used in microcapsules placed inside textile fibres, which absorb, store and release

energy in a reactive way to warm in cold or cool when it is hot. The PCM intervene to regulate heat transfer between the body and the outside.

In order to simulate numerically the temporal evolution of charge and discharge energy in PCM, most of the studies are linked to:

- First, a simplified hypothesis, assuming a constant and uniform heat transfer coefficient along the different interfaces of change phase and using quasi-steady-state models. These studies use correlations for heat transfer coefficients during freezing and melting.
- Second, studies that do not take into account natural convection (Cao and Faghri, 1991) assuming that heat transfer during the charge process is only due to conduction.
- Third, studies that consider the whole phase change phenomenon, e.g. natural convection and conduction (Cao and Faghri, 1991; Bejan, 1996; Badar and Zubair, 1995; Mithal and Yang, 1994; Charach and Conti, 1995). Most of them are based on optimization procedures. Because of the problem complexity, the interface that separate different phases is not determine with good accuracy.

Many experimental and numerical studies have been dedicated to convection-dominated melting of PCM for various geometries, e.g. along a vertical wall, inside as well as around a horizontal cylinder, etc. The situation of a PCM heated from below was also the subject of numerical works. We can mention, for example, the studies of Gong and Mujumdar (1998), Kousksou *et al.* (2010), Wintruff *et al.* (2001), Fteiti and Nasrallah (2004) and Jellouli *et al.* (2007). Experimental works, such as Dietsche and Müller (1985) surveys have also been devoted to this case.

One could ask the question: does a practical reason exist to why one might want to melt or to cool a PCM from below as opposed to from the side or above? Indeed, the melting of a pure PCM in a rectangular container heated from below is used also to control the temperature of the surface of electronic or electric components that release instantaneous or periodic high-density heat flux, in order to moderate the need of classical cooling devices. There has been an increasing interest for this type of passive cooling when applied for electronic circuits as chipsets, processors of laptops or graphics cards. These elements are continuously miniaturized and their heat release densities are increasing, therefore, they require high performance but economic and silent cooling systems. Often, the geometric disposition of the electronic component surfaces requires a cooling from below. Sometimes, the heating or cooling from below is necessary or more efficient on account of the electric or electronic environment.

It is well known that when a horizontal layer of fluid is heated from below, a cellular form of natural convection may occur inside the liquid, similar to that observed during classical Rayleigh-Bénard convection. As a result of the interaction between the cellular convection and the melting process, the phase-change interface, which is assumed to be at the equilibrium temperature, tends to get wavy. Yen and Galea (1968), Yen (1980) and Seki *et al.* (1977) experimentally studied the melting of a horizontal ice slab heated from below. Hale and Viskanta (1980) performed experiments for melting from below and solidification from top of *n*-octadecane in a rectangular cavity. They did not present flow patterns and phase change interface shapes, however, Gau *et al.* (1983) presented flow visualization for melting from below of a *n*-octadecane slab in a rectangular cavity. Diaz and Viscanta (1984) extended the experiments of Gau *et al.* (1983) to morphology observation of the liquid-solid interface. To study the melting

of a pure PCM in a rectangular container heated from below, Gong and Mujumdar (1998) used the Streamline Upwind/Petrov Galerkin finite element in combination with a fixed grid primitive variable method.

In the present paper we propose a high-accuracy model of the melting process in a rectangular cavity heated from below, with a good approximation of the time evolution of the liquid-solid interface. In the first stage of this work, we consider the dynamic and thermal energy storage process of a PCM subjected to a uniform and constant heat flux or wall temperature. In a second paper, the PCM will be submitted to a pulsed heated flow located at the bottom of the PCM cavity.

A single cell is analysed to understand the mechanism of an entire system of cells. The PCM is considered confined in a closed area, whose sidewalls are thermally insulated, and whose lower wall is heated at constant and uniform temperature or heat flux. During the charge and discharge time process, the material in the cell is in one or two phases, solid/liquid. The interface separating the two phases is a critical unknown of the problem. The unsteady dynamic and thermal phenomena will be presented and discussed. In view to validate the present study, Section 9.4 is devoted to the comparison between the present model results and some Benchmark solutions proposed, for example, by Rubinstein (1971) (analytical survey), Wintruff *et al.* (2001) (numerical validation of Dietsche and Müller, 1985 experimental work) or Gong and Mujumdar (1998) (numerical study).

From a numerical point of view, the Navier-Stokes equations written in  $(\omega-\psi)$  formulation and the energy equation are solved in space by spectral collocation methods (Canuto *et al.*, 1988; Bernardi and Maday, 1992; Gelfgat, 2004; Shen, 1994, 1995, 1997). The resolution in time is carried out by Crank-Nicolson scheme.

This work can be summarized as follows: in the first section, we give governing equations and boundary conditions associated to the physical model. Next, we describe the spectral numerical method to solve these equations. Then the numerical studies focus on the thermal problem and its associated heat transfer. Finally in the last section, numerical results obtained are analysed in the following order: study of the dynamic and thermal fields, evolution of the interface solid-liquid, convergence of results according to numerical parameters, validation tests. A discussion is given in conclusion.

## 2. Hypotheses and governing equations

We consider a two-dimensional (2D) section of a cell in Cartesian coordinates. Lateral vertical walls are supposed to be parallel to the  $y$ -axis; in contrast, bottom and top walls can be of any shape, defined by the shape functions  $H_L$  and  $H_S$  (Figure 1).

The material confined in this cell presents one or two phases: solid and/or liquid. So, at each time  $t > 0$ , we have to solve the following problems:

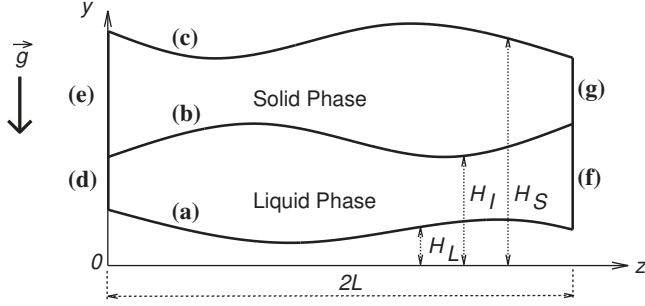
### *Solid phase*

In the solid domain, we solve the diffusion equation:

$$\rho_S C_{P_S} \left( \frac{\partial \theta_S}{\partial t} + u \frac{\partial \theta_S}{\partial z} + v \frac{\partial \theta_S}{\partial y} \right) = \lambda_S \left( \frac{\partial^2 \theta_S}{\partial z^2} + \frac{\partial^2 \theta_S}{\partial y^2} \right) \quad (1)$$

### *Liquid phase*

The temperature differences are assumed sufficiently low to justify the Boussinesq approximation in the liquid phase flow of the PCM. The fluid is assumed Newtonian



**Notes:** (a) Cell bottom wall; (b) interface solid/liquid; (c) cell top wall; (d), (e), (f) and (g) vertical walls

and isotropic, and we suppose that the flow is laminar and incompressible. With the 2D hypothesis, we use the vorticity-stream function formulation  $(\omega, \psi)$  for the Navier-Stokes equations in which the incompressibility condition is automatically satisfied. In fact, the essential advantage of this formulation compared to the primitive variables (velocity-pressure formulation) is the reduction of the number of unknown functions and the non-used of the pressure. On the other hand, Navier-Stokes equations become a fourth-order Partial Differential Equations whose expressions in Cartesian coordinates are:

$$\frac{\partial \omega}{\partial t} - \frac{\partial \psi}{\partial z} \frac{\partial \omega}{\partial y} + \frac{\partial \psi}{\partial y} \frac{\partial \omega}{\partial z} = \nu \left( \frac{\partial^2 \omega}{\partial y^2} + \frac{\partial^2 \omega}{\partial z^2} \right) - g\beta \frac{\partial \theta_L}{\partial z} \quad (2)$$

It is important to note that we have only one unknown function, e.g.:  $\psi$ . The vorticity function  $\omega$  is linked to  $\psi$  by the relation:

$$\omega = - \left( \frac{\partial^2 \psi}{\partial z^2} + \frac{\partial^2 \psi}{\partial y^2} \right) = -\Delta \psi \quad (3)$$

The energy equation is given by:

$$\rho_L C_{P_L} \left( \frac{\partial \theta_L}{\partial t} + u \frac{\partial \theta_L}{\partial z} + v \frac{\partial \theta_L}{\partial y} \right) = \lambda_L \left( \frac{\partial^2 \theta_L}{\partial y^2} + \frac{\partial^2 \theta_L}{\partial z^2} \right) \quad (4)$$

The expressions of velocity components are:

$$u = \frac{\partial \psi}{\partial y} \quad \text{and} \quad v = - \frac{\partial \psi}{\partial z} \quad (5)$$

#### *Interface solid/liquid*

The temporal evolution of the interface solid-liquid height  $H_I(x, t)$  is given by Guerrero *et al.* (1999):

$$\rho_S La \frac{\partial H_I}{\partial t} = \frac{\alpha_I}{\sqrt{1 + \left( \frac{\partial H_I}{\partial z} \right)^2}} \quad (6)$$

where  $\alpha_I$  traduces the heat transfer between the solid and liquid phases along the interface:

$$\alpha_I = \lambda_L \left( \frac{\partial \theta_L}{\partial y} \right)_I - \lambda_S \left( \frac{\partial \theta_S}{\partial y} \right)_I \quad (7)$$

### 3. Boundary conditions

At any time  $t > 0$ , all unknown functions must verify the imposed boundary conditions. There are two types of boundary conditions: those related to the solid phase and those associated to the liquid phase. According to Figure 1, they can be summarized as follows.

#### *Interface solid/liquid*

On the interface solid/liquid (b), the temperature is equal to the melting temperature of the PCM:  $\theta = \theta_M$ .

#### *Solid phase*

*Thermal conditions.* Vertical walls (e)-(g) are thermally insulated, then the temperature normal derivative is equal to 0:  $\frac{\partial \theta}{\partial n} = 0$ .

#### *Liquid phase*

*Thermal conditions:*

- As for solid phase, vertical walls (d)-(f) are thermally insulated, then we have:  $\frac{\partial \theta}{\partial n} = 0$
- The bottom wall (a) is submitted to a constant and uniform given temperature  $\theta_W$ ,  $\theta = \theta_W$  or to a constant and uniform given heat flux  $\Phi_W$ ,  $-\lambda \frac{\partial \theta}{\partial n} = \Phi_W$

*Dynamic conditions.* For reasons of simplicity, the dynamic conditions will deal with velocity, and one can deduce easily the corresponding boundary conditions on the stream function  $\psi$ .

We impose:  $u = v = 0$  on all solid boundaries of the liquid domain (a)-(b)-(d)-(f).

### 4. Variables transformations

Each problem is solved by spectral collocation method. Consequently, each study domain is to be transformed into square  $[-1, 1] \times [-1, 1]$ . In order to obtain this computational square domain permitting the use of 2D Chebyshev polynomials, we carry out the space variables Landau transformation  $L$  (Canuto *et al.*, 1988; Jellouli *et al.*, 2007; Batina *et al.*, 2011). We summarize this method below.

For many 2D problems, the geometry of study is a complex domain shape. For periodic geometries (Batina *et al.*, 2009, 2011), the upper and lower walls are periodic functions of the variable  $z$ . In order to deal with such geometries, we consider a general 2D-domain ( $D$ ) as shown on Figure 2, with lateral edges parallel to  $y$ -axis; the two other vertical edges are defined by functions  $a(z)$  and  $b(z)$ .

Let us take any abscise  $z \in [0, 2L]$ , and assume that  $(z, y) \in (D)$ .

First,  $y$  must verify:  $a(z) \leq y \leq b(z)$ . Second, we define the Landau variable transformations  $L$ :

$$(x, r) = L(z, y), \text{ with: } \begin{cases} x = \frac{z}{L} - 1 \\ r = \frac{1}{h(z)} [y - k(z)] \end{cases} \quad (8)$$

where:

$$\begin{cases} h(z) = \frac{b(z)-a(z)}{2} \\ k(z) = \frac{b(z)+a(z)}{2} \end{cases} \quad (9)$$

Then, the primary domain ( $D$ ) is transformed into the square domain  $-1 \leq x \leq 1$  and  $-1 \leq r \leq 1$ . Note that it may be easier to follow the Landau transformation if only the phase front height was a function of  $z$ .

### 5. New system of governing equations

According to variables transformation (8), we have to rewrite the new system of governing equations.

#### Energy equations

The energy equations become:

$$Lh^2\theta + h^2u \frac{\partial \theta}{\partial x} + h[vL - (rh' + k')u] \frac{\partial \theta}{\partial r} = \frac{\lambda}{\rho LC_P} \Delta_f \theta \quad (10)$$

where  $\Delta_f \theta$  represents the expression:

$$\Delta_f \theta = A_f(x, r) \frac{\partial^2 \theta}{\partial x^2} + B_f(x, r) \frac{\partial^2 \theta}{\partial r^2} + C_f(x, r) \frac{\partial \theta}{\partial r} + D_f(x, r) \frac{\partial^2 \theta}{\partial x \partial r} \quad (11)$$

with:

$$A_f(x, r) = h^2; B_f(x, r) = L^2 + (rh' + k')^2; \quad (12)$$

$$C_f(x, r) = 2(rh'^2 + k'h') - h(rh'' + k''); D_f(x, r) = -2(rhh' + hk')$$

Note that all derivatives like  $h'$  or  $k'$  are relative to the new variable  $x$ , e.g.:

$$h' = \frac{dh}{dx} = L \frac{dh}{dz} \text{ and } k' = \frac{dk}{dx} = L \frac{dk}{dz} \quad (13)$$

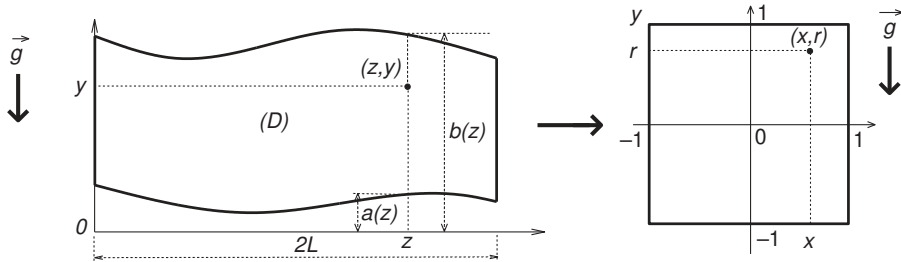


**Figure 2.** Space variables Landau transformation  $L$  on a general 2D-domain ( $D$ )

These equations are available for the both phases solid and liquid. Explicitly, for:  
Solid phase, we have:

$$u = v = 0 \text{ and } \begin{cases} h_S = \frac{H_S - H_I}{2} \\ k_S = \frac{H_S + H_I}{2} \end{cases} \quad (14)$$

Liquid phase, one has:

$$\begin{cases} h_L = \frac{H_I - H_L}{2} \\ k_L = \frac{H_I + H_L}{2} \end{cases} \quad (15)$$

*Navier-Stokes equations*

For reasons of clarity, the subscript  $L$  will be omitted in the functions  $h_L$  and  $k_L$ .  
With the above variables transformations, the Navier-Stokes equations become in the liquid phase:

$$\begin{aligned} Lh^2 \frac{\partial \check{\omega}}{\partial t} + h \left( \frac{\partial \psi}{\partial r} \frac{\partial \check{\omega}}{\partial x} - \frac{\partial \psi}{\partial x} \frac{\partial \check{\omega}}{\partial r} \right) - 2h' \frac{\partial \psi}{\partial r} \check{\omega} \\ = \widehat{v} \Delta_g \check{\omega} - g\beta L^2 h^2 \left( h^2 \frac{\partial \theta}{\partial x} - h(\rho h' + k') \frac{\partial \theta}{\partial r} \right) \end{aligned} \quad (16)$$

where:

$$\widehat{v} = \frac{v}{L} \quad (17)$$

$$\Delta_g \check{\omega} = A_g \frac{\partial^2 \check{\omega}}{\partial x^2} + B_g \frac{\partial \check{\omega}}{\partial r^2} + C_g \frac{\partial \check{\omega}}{\partial r} + D_g \left( \frac{\partial^2 \check{\omega}}{\partial x \partial r} \right) + E_g \frac{\partial \check{\omega}}{\partial x} + F_g \check{\omega} \quad (18)$$

$$\begin{cases} A_g = h^2; B_g = L^2 + (rh' + k')^2; C_g = -h(rh'' + k'') + 6h'(rh' + k') \\ D_g = -2(rhh' + hk'); E_g = -4hh'; F_g = 2(3h^2 - hh'') \end{cases} \quad (19)$$

The new vorticity function  $\check{\omega}$  is written by the mean of the stream function  $\psi$  as follows:

$$\check{\omega} = L^2 h^2 \omega = -\Delta_f \psi \quad (20)$$

The operator  $\Delta_f$  is given by the relations (11)-(12), and the heights  $h$  and  $k$  are relative to liquid phase (Equation (15)).

After division by  $Lh^2$ , Equation (10) can take the following form:

$$\frac{\partial \check{\omega}(x, r; t)}{\partial t} = f(\check{\omega}) \quad (21)$$

with:

$$f(\check{\omega}) = - \left[ \frac{1}{Lh} \left( \frac{\partial \psi}{\partial r} \frac{\partial \check{\omega}}{\partial x} - \frac{\partial \psi}{\partial x} \frac{\partial \check{\omega}}{\partial r} \right) - \frac{2}{Lh^2} \left( h' \frac{\partial \psi}{\partial r} \right) \check{\omega} \right] + \frac{\widehat{v}}{Lh^2} \Delta_g \check{\omega} + S_T \quad (22)$$

where  $S_T$  is the source term:

$$S_T = -Lg\beta \left( h^2 \frac{\partial \theta}{\partial x} - h(rh' + k') \frac{\partial \theta}{\partial r} \right) \quad (23)$$

## 6. Numerical resolution of the dynamic problem

### 6.1. Time-integration using Crank-Nicolson scheme

We need a time-integration scheme to solve Equation (21). We chose the  $\varepsilon$ -method, reduced here to Crank-Nicolson method corresponding to  $\varepsilon = 1/2$ . The main advantages of this method are its unconditional stability and its second-order accuracy. It leads to the scheme below:

$$\begin{cases} \frac{\check{\omega}^{n+1} - \check{\omega}^n}{\Delta t} = \varepsilon f(\check{\omega}^{n+1}) + (1 - \varepsilon) f(\check{\omega}^n) \\ \check{\omega}^n = -\Delta_f \psi^n, \forall n \end{cases} \quad (24)$$

where  $\Delta t$  is a given time step and  $n \geq 0$  is the time step number. The initial condition  $\psi^0$  is taken here equal to 0 on the whole domain of study.

### 6.2 Space-resolution using spectral collocation method

**6.2.1 Trial functions and development orders.** The spectral methods consist in projecting any unknown function  $\varphi(x, r, t)$  on trial functions as follows:

$$\varphi(x, r, t) = \sum_{k=0}^{N_x} \sum_{l=0}^{N_r} \varphi_{kl}(t) P_l(r) Q_k(x) \quad (25)$$

where  $N_x$  and  $N_r$  are the development orders according to the axis  $x$  and  $r$ , respectively (Batina *et al.*, 2009). The bases functions  $P_l(r)$  and  $Q_k(x)$  are generally trigonometric or polynomial (Chebyshev, Legendre, etc.) according to boundary conditions situations. The time dependant coefficients  $\varphi_{kl}(t)$  are the unknowns of the problem. For our equations, the function  $\varphi$  represents  $\psi$  or  $\theta$ .

Note that it is necessary to study the influence of the physical parameters such as the Raleigh number to remain in 2D hypothesis. From a numerical point of view, we will show the influence of the polynomials degrees particularly for the thermal problem.

**6.2.2 The choice of bases functions.** Because no symmetry condition is imposed at the boundaries of our domain of study, we choose bases functions constructed from Chebyshev polynomials (Bernardi and Maday, 1992; Canuto *et al.*, 1988) instead of trigonometric trial functions. Then,  $P_l(r)$  and  $Q_k(x)$  are written as linear combination of Chebyshev polynomials. Their expressions depend on the boundary conditions. According to Gelfgat (2004) and Shen (1994, 1995, 1997), we set:

$$P_l(r) = T_l(r) + \sum_{i=1}^n \alpha_i T_{l+i}(r) \text{ and } Q_k(x) = T_k(x) + \sum_{i=1}^m \beta_i T_{k+i}(x) \quad (26)$$

where  $n$  (respectively  $m$ ) is the number of boundary conditions according to the vertical direction  $r$  (respectively the axial direction  $x$ ) and  $T_k$  is the Chebyshev polynomial of degree  $k$ .

6.2.3 *The stream function spectral development.* According to the general formulation (25), the stream-function  $\psi$  is projected on trial functions as follows:

$$\psi(x, r) = \sum_{k=0}^{N_x} \sum_{l=0}^{N_r} \psi_{kl} P_l(r) Q_k(x) \quad (27)$$

The Chebyshev polynomials  $P_l(r)$  and  $Q_k(x)$  are given by (26). Because of the condition  $u = v = 0$  on all solid boundaries and the flow-rate conservation condition, we have:

$$P'_l(r) = P_l(r) = 0 \text{ at } r = \pm 1 \text{ and } Q'_k(x) = Q_k(x) = 0 \text{ at } x = \pm 1 \quad (28)$$

The Neumann conditions are taken into account in the expressions of  $P_l(r)$  and  $Q_k(x)$ , but the Dirichlet conditions are introduced directly in the matrix systems. So, we have  $n = m = 2$ . Finally, one can determine all coefficients  $\alpha_l$  and  $\beta_k$  in Equations (26). We obtain:

$$\begin{cases} P_l(r) = T_l(r) - \frac{l^2}{(l+2)^2} T_{l+2}(r) \\ Q_k(x) = T_k(x) - \frac{k^2}{(k+2)^2} T_{k+2}(x) \end{cases} \quad (29)$$

The vorticity function can be written as follows:

$$\tilde{\omega} = \sum_{k=0}^{N_x} \sum_{l=0}^{N_r} A_{kl}(x, r) \psi_{kl} \quad (30)$$

where:

$$\begin{cases} A_{kl}(x, r) = \alpha_f P_l(r) Q'_k(x) + \beta_f P'_l(r) Q_k(x) + \gamma_f P'_l(r) Q_k(x) + \delta_f P'_l(r) Q'_k(x) \\ \alpha_f = h^2; \beta_f = r^2 + r^2 h'^2; \gamma_f = r(2h'^2 - hh''); \delta_f = -2rhh' \end{cases} \quad (31)$$

6.2.4 *The spectral collocation method.* The collocation method consists to write the equation (24) on specific points  $(x = x_i, r = r_j)_{\substack{0 \leq i \leq N_x \\ 0 \leq j \leq N_r}}$  of the square  $[-1, 1] \times [-1, 1]$ ,

called collocation points:  $(N_x + 1)$  points according to the axial direction  $x$  and  $(N_r + 1)$  points according to the vertical direction  $r$ . We chose the collocation points of Chebyshev-Gauss-Lobatto (Batina *et al.*, 2009, 2011), defined by:

$$x_i = -\cos(i\pi/N_x) \text{ and } r_j = -\cos(j\pi/N_r) \quad (32)$$

with  $0 \leq i \leq N_x$  and  $0 \leq j \leq N_r$

Then, the Navier-Stokes Equation (24) is written at each collocation point ( $x = x_i$ ) and ( $r = r_j$ ). At last, we have to solve the non-linear system:

$$F_{ij}(\check{\omega}) = -\check{\omega}_{i,j}^{n+1} + \frac{\Delta t}{2} f(\check{\omega}_{i,j}^{n+1}) + S_{i,j} = 0 \quad (33)$$

with  $S_{i,j}$  the source term given by:

$$S_{i,j} = \left\{ \check{\omega}_{i,j}^n + \frac{\Delta t}{2} f(\check{\omega}_{i,j}^n) \right\} \quad (34)$$

$$\check{\omega}_{i,j}^s = \sum_{k=0}^{N_x} \sum_{l=0}^{N_r} A_{kl}(x_i, r_j) \psi_{kl}^s \quad (35)$$

where  $s = n$  or  $s = n + 1$  is the time-step number.

At each time step, the unknowns  $\psi_{kl}$  are obtained by solving the non-linear system (33) with Newton algorithm.

## 7. Numerical resolution of the thermal problem

### 7.1 Choices of the bases functions

The choice of the temperature bases functions is made in the same way as in the dynamic problem. The temperature  $\theta$ , truncated at development orders  $N_x$  according to the axis  $x$  and  $N_r$  according to the radius  $r$ , is projected on the trial functions as follows:

$$\theta(x, r, t) = \sum_{k=0}^{N_x} \sum_{l=0}^{N_r} \theta_{kl}(t) q_k(x) p_l(r) \quad (36)$$

where  $p_l(r)$  and  $q_k(x)$  are built from Chebyshev polynomials as in Section 5. According to temperature boundary conditions, we obtain at last:

$$q_k(x) = T_k(x) \text{ and } p_l(r) = T_l(r) \quad (37)$$

### 7.2 Resolution of the thermal unsteady problem

The thermal Equation (10) is numerically integrated in time by using the second-order Crank-Nicolson scheme in the same way as in the dynamic problem.

By projecting Equation (10) in the collocation basis  $(q_k(x) p_l(r))_{ij}$ , one obtains at each time step a system of linear equations solved by the classical Gauss method.

## 8. Convective heat transfer

In view to analyse the influence of the PCM melting process on the cell bottom wall heat transfer, especially during the convective phase, we introduce the local convective heat transfer coefficient  $\tau_W$  as follows:

$$\tau_W(x, t) = \frac{\Phi_W}{\Delta\theta_{ref}} \quad (38)$$

where  $\Delta\theta_{ref}$  is a typical difference temperature reference. That one depends on the wall boundary conditions hypotheses. The main difficulty with convective unsteady heat transfer lies in the temperature reference choice. Because the PCM cell is heated from below and with the presence of the liquid phase, we have chosen:

$$\Delta\theta_{ref} = \bar{\theta}_W - \theta_M \quad (39)$$

where  $\bar{\theta}_W$  is the space-averaged bottom wall temperature, given by the curvilinear integral:

$$\bar{\theta}_W = \frac{1}{L_W} \int_{BottomWall} \theta(M) dM \quad (40)$$

with  $L_W$  the curvilinear length of the bottom wall. One can notice that  $\Delta\theta_{ref}$  is generally time-dependent, except when the bottom wall is heated at constant temperature.

So, the instantaneous convective heat transfer at the cell bottom wall can formally be defined by the local Nusselt number  $Nu_W(x, t)$  based on the half thickness  $h_L = (H_I - H_L)/2$  of the liquid domain. Its expression is given by the relation:

$$Nu_W(x, t) = \frac{h_L(x, t)\tau_W(x, t)}{\lambda_L} \quad (41)$$

With the variables transform (Section 4), we have:

$$\Phi_W = \lambda_L \frac{\sqrt{1 + (H'_L)^2}}{h_L} \left\{ - \left( \frac{\partial\theta}{\partial r} \right)_W + \frac{h_L H'_L}{L(1 + (H'_L)^2)} \left( \frac{\partial\theta}{\partial x} \right)_W \right\} \quad (42)$$

Then, the Nusselt number can be written as follows:

$$Nu_W(x, t) = \frac{\sqrt{1 + (H'_L)^2}}{\Delta\theta_{ref}} \left\{ - \left( \frac{\partial\theta}{\partial r} \right)_W + \frac{h_L H'_L}{L(1 + (H'_L)^2)} \left( \frac{\partial\theta}{\partial x} \right)_W \right\} \quad (43)$$

## 9. Numerical results

### 9.1 Initial conditions and numerical parameters

The results presented below correspond to a PCM whose physical properties are similar to water properties (determined at a mean temperature equal to 10°C), initially in the form of an ice block (Figure 3) at a uniform temperature  $\theta_{S_0} = -1^\circ\text{C}$ , and whose 2D rectangular dimensions are: *Length* =  $2L = 2 \cdot 10^{-2}\text{m}$  and *Height* =  $H_S = 10^{-2}\text{m}$ . We assumed that the coefficient of thermal expansion  $\beta$  is temperature free. At time  $t = 0$ , the cell lower wall is heated to a uniform temperature  $\theta_W = 10^\circ\text{C}$ , the other walls of the cell (top wall and vertical walls) are assumed to be adiabatic.

Note that this work focused on the numerical analysis of the melting process inside a 2D cavity by using the spectral collocation method. To simplify the present study, we

have considered that the density varies linearly with temperature. Numerical analysis shows that all parameters, time-steps and polynomials developments orders are linked and have to be chosen carefully to assume optimal accuracy results. Unlike normal liquid PCMs, pure water exhibits maximum density near 4°C at atmospheric pressure. In such case, the problem becomes even more complex because the assumption that the density varies linearly with temperature cannot be applied. Future work will focus on that issue.

Moreover, to avoid numerical aberration at the instant  $t = 0$ , we suppose that:

- (1) There exists initially a very few quantity of liquid, of height  $H_{L_0} = 10^{-3}\text{m}$ , at initial uniform temperature  $\theta_{L_0} = 0^\circ\text{C}$ , parallel to the cell lower wall (Figure 3).
- (2) The uniform temperature or heat flux imposed to the heated bottom wall is reached gradually, from zero to the imposed value, within a short time interval, less or equal to ten seconds. Therefore, all results are analysed since this moment.

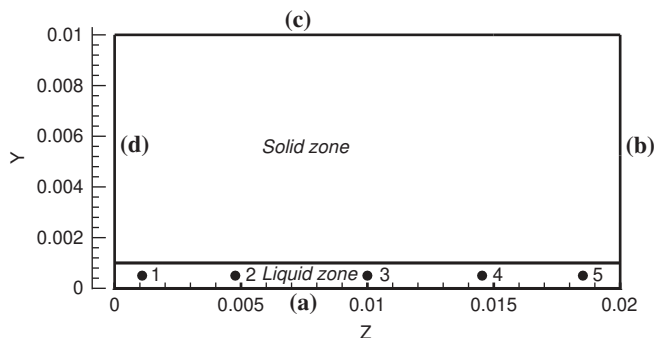
In order to follow the temporal evolution of the thermal field, particular control points are chosen in the study domain as shown in Figure 3. We chose five control points situated to the mid-height of the liquid phase and symmetrical in relation to the central Point 3 and whose abscissas are, respectively: Point 1:  $x_1 = L/8$ ; Point 2:  $x_2 = L/2$ ; Point 3:  $x_3 = L$ .

The computations were performed with suitable orders of Chebyshev polynomials developments and an optimal time step  $\Delta t$ . We present the results obtained with  $N_x = 62$ ,  $N_r = 18$  and  $\Delta t = 0.2\text{s}$ . A discussion concerning numerical results accuracy and convergence according to those different truncature orders and time steps will be presented farther, at the end of this chapter.

Note that the melting process into the PCM cell is governed by three classical dimensionless numbers: the instantaneous Rayleigh number  $Ra(t)$  based on the mean thickness  $H_m(t)$  of the liquid layer, the Prandtl number  $Pr$  and the Stephan number  $Ste$ :

$$Ra(t) = \frac{g\beta H_m^3(t)(\theta_w - \theta_M)}{a_L \nu} \quad (44)$$

$$Pr = \frac{\nu}{a_L} \quad (45)$$



**Notes:** (a) Cell bottom wall:  $\theta = \theta_w = 20^\circ\text{C}$ ; (b), (c) and (d) adiabatic vertical walls 1-5, control points

**Figure 3.** Initial conditions in the PCM cell with a few liquid phase and a solid phase

$$Ste = \frac{C_{PL}(\theta_W - \theta_M)}{La} \quad (46)$$

with  $a_L$  the liquid thermal diffusivity:

$$a_L = \frac{\lambda_L}{\rho_L C_{PL}} \quad (47)$$

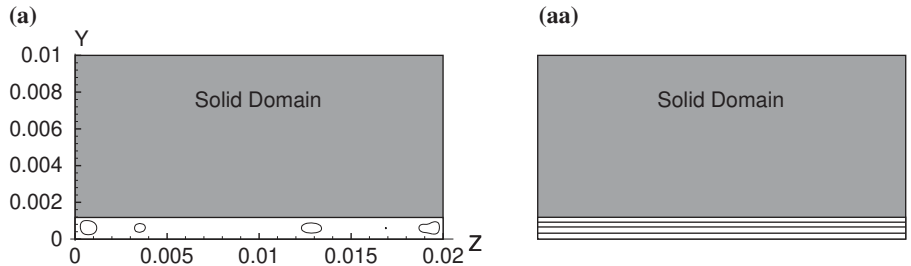
For our problem, one has:  $Pr = 9.40$  and  $Ste = 0.23$ . The instantaneous Rayleigh number is crucial to determine the critical threshold of convection apparition in the liquid phase. We analyse below the evolution of dynamic and thermal field in the PCM as a function of the temperature imposed on the heated cell lower wall, the temporal variation of Nusselt number and the evolution of liquid-solid interface.

## 9.2 The PCM melting process

**9.2.1 Notations used for the streamlines and the isotherms.** About the streamlines and the isotherms, we define on each figure the following parameters:  $N_\psi$  the number of streamlines,  $N_\theta$  the number of isotherms,  $\psi_{min}$  and  $\psi_{max}$  the minimum value and the maximum value of the stream function  $\psi$ , respectively,  $\theta_{min}$  and  $\theta_{max}$  the minimum value and the maximum value of the temperature  $\theta$ , respectively. The step size from the minimum value to the maximum value is chosen constant. For streamlines, we indicate the direction of rotation of the first vortex located leftmost.

**9.2.2 The conductive phase.** At the beginning of the PCM melting process, when the liquid phase appears, the heat transfer in the cell is governed only by conduction phenomenon. The liquid-solid interface remains straight and parallel to the cell lower wall. The isotherms are straight lines, as we can verify it in Figure 4 that presents the instantaneous streamlines and isotherms. No flow is detected in the liquid region except a very small residue, of the order of  $10^{-16}$ , situated close to the left and to the right lower wall corners.

The fluid layers adjacent to the interface, colder and denser, are located above warmer and lighter layers situated in the vicinity of the cell lower wall. This is a potentially unstable stratification, which represents essentially the classic problem of Rayleigh-Bénard. As long as the temperature gradient in the cell remains purely vertical, the Boussinesq source expression  $(\partial\theta_L)/(\partial z)$  in the Navier-Stokes Equation (2) is equal to zero.



**Notes:**  $N_\psi = 14$ ,  $\Psi_{min} = -9.10^{-7}$ ,  $\Psi_{max} = 9.10^{-7}$ ;  $N_\theta = 4$ ,  $\theta_{min} = 0^\circ\text{C}$ ,  $\theta_{max} = 6.7^\circ\text{C}$

**Figure 4.** (a) Temporal evolution of streamlines and (aa) corresponding isotherms in conductive phase, at time  $t = 20$  s

9.2.3 *The convective phase.* As the interface height increases, the Rayleigh number  $Ra$  grows with the thickness of the liquid layer. Stratification becomes unstable when  $Ra$  reaches the critical threshold of  $Ra_{crit} = 4,575$  representing the higher limit of the pure conduction regime without flow, so that any slightest mechanical or thermal disturbance amplifies and initiates the convection phenomenon by breaking the horizontal thermal equilibrium.

In Figure 5, we note that the presence of the flow distorts the isotherms, but the interface remains still straight for a moment before starting to warp as a result of the temperature non-uniformity due to the presence of convective vortex. It is interesting to notice that to the beginning of the interface distortion, at time  $t = 330$  s, there were seven Bernard-vortexes in the liquid region whose rotation alternates from one to another. We observe that the dynamics of these vortexes is the consequence of the liquid fraction increasing, and thus the dynamics of the interface evolution. This phenomenon is due to the rotation of convection vortexes, forcing the liquid to absorb heat along the bottom wall of the cell before transferring this energy to the interface. A qualitative comparison shows that these results are in good agreement with the literature survey, those obtained by Guerrero *et al.* (1999), for example. As time increases, the number of convective vortexes in the cavity decreases gradually.

The temporal evolution of the PCM interface solid/liquid (Figure 6) confirms the transition from conductive to convective phase: the interface remains straight in conductive region, before starting to warp under the convective vortexes influence, at  $t \approx 330$  s.

Figure 7 shows the time evolution of the Rayleigh number. After a regular evolution, we observe a sudden changing behaviour related to the presence of convective vortexes. We deduce that we reach the critical Rayleigh number  $Ra_{crit}$ , and we obtain with this Figure 7:

$$Ra_{crit} = 4,575 \quad (48)$$

So, with this critical Rayleigh number value, one can deduce the corresponding critical mean thickness value of the fluid layer  $H_{crit}$ :

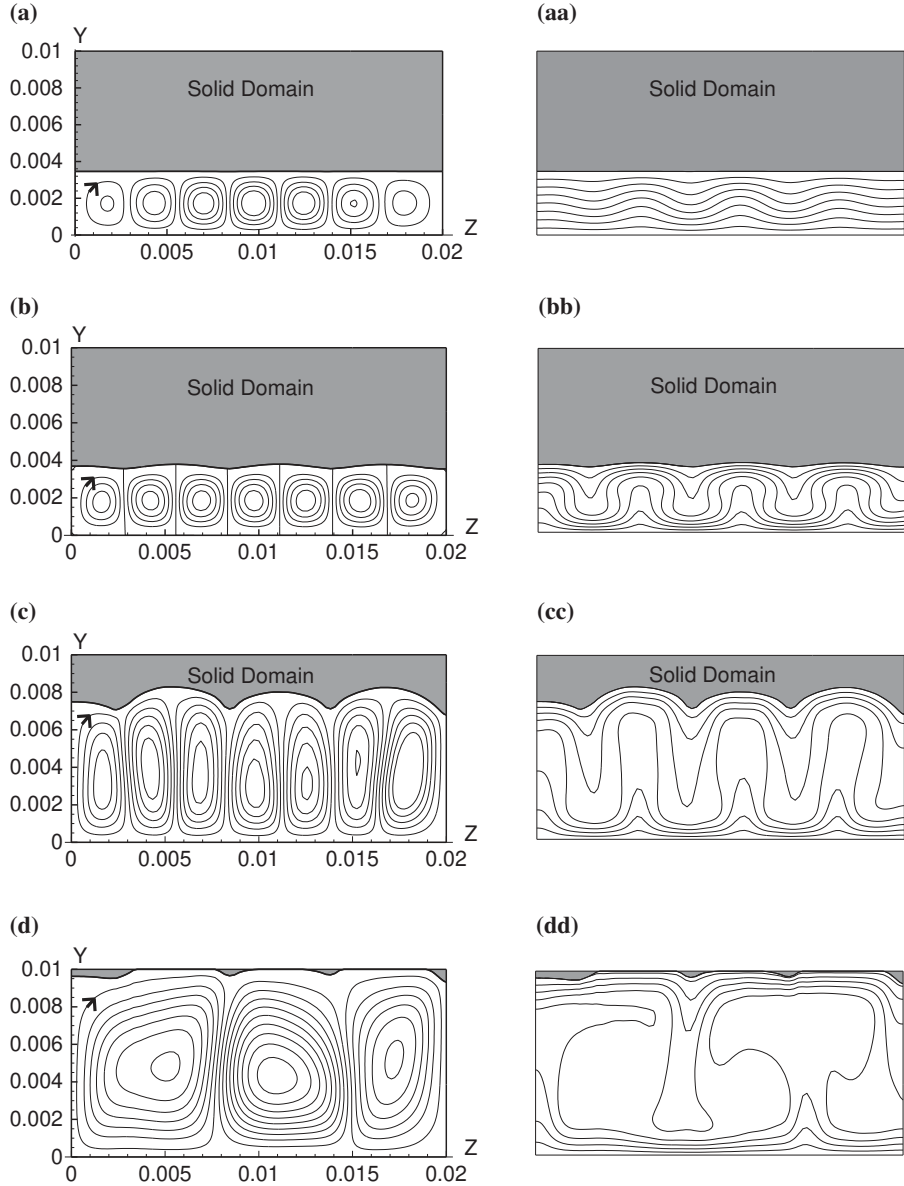
$$H_{crit} = \sqrt[3]{\frac{a_L \nu Ra_{crit}}{g\beta(\theta_W - \theta_M)}} \approx 3.46 \cdot 10^{-3} \text{m} \quad (49)$$

This value corresponds to the value obtained with Figure 6, and is reached at the time:

$$t = t_{crit} \approx 330 \text{s} \quad (50)$$

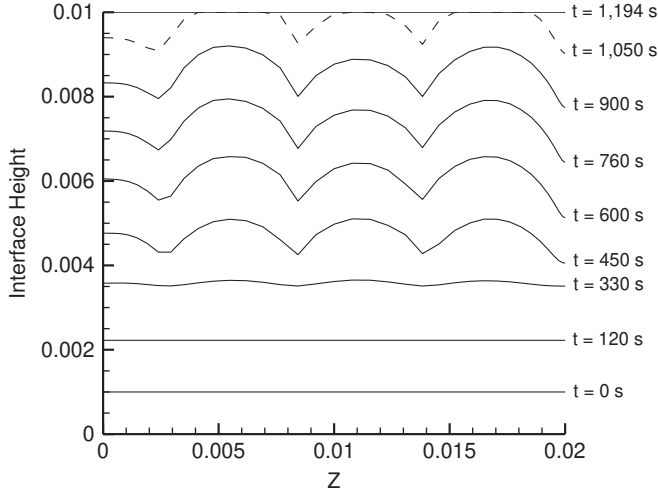
We also clearly notice an increase of  $Ra(t)$  in the convective regime, accompanied by a decrease of vortexes number in the liquid phase. The maximum value  $Ra_{max} = 108,990$  of  $Ra(t)$  is reached at the melting process end, at the time  $t = t_{end} \approx 1,190$  s. Past this time, the Rayleigh number is constant.

Figure 7 shows also the Nusselt number temporal evolution at the bottom of the cavity. In conductive regime, the Nusselt number is constant:  $Nu(t) = 0.54$ . This behaviour is typical of all problems related to phase change dominated by conduction. An abrupt transition from conductive to convective regime at  $t = 330$  s is clearly visible on this figure. As for Rayleigh number behaviour, we observe an increase of  $Nu(t)$  in



**Notes:** (a)  $t = 316$  s,  $N_\psi = 8$ ,  $\Psi_{min} = -2.10^{-7}$ ,  $\Psi_{max} = 2.10^{-7}$ ; (b)  $t = 340$  s,  $N_\psi = 15$ ,  $\Psi_{min} = -1.10^{-6}$ ,  $\Psi_{max} = 1.10^{-6}$ ; (c)  $t = 790$  s,  $N_\psi = 10$ ,  $\Psi_{min} = -8.10^{-7}$ ,  $\Psi_{max} = 8.10^{-7}$ ;

**Figure 5.** Snapshots of streamlines (a, b, c, d) and corresponding isotherms (aa, bb, cc, dd) in convective phase



**Figure 6.** Temporal evolution of the PCM interface solid/liquid

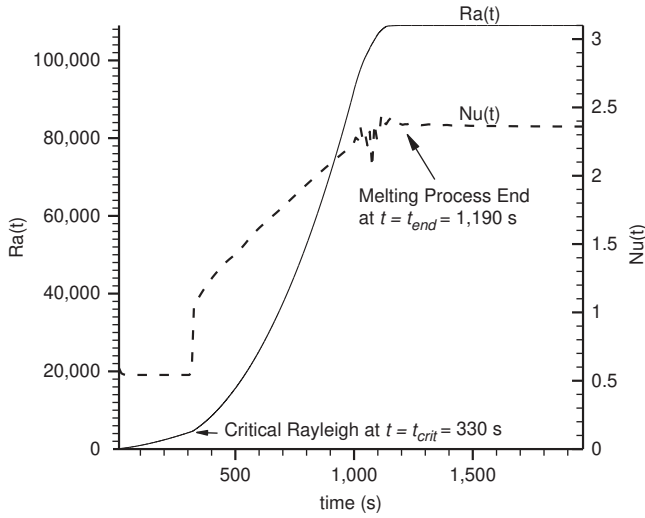


**Figure 7.** Temporal evolution of the Rayleigh number and the Nusselt number

the convective regime, with a maximum value  $Nu_{max} = 2.38$  reached at the melting process end time  $t = t_{end} \approx 1,190$  s, followed by a constant time-evolution.

The total (reduced) thermal energy in the PCM is given by:

$$E_{tot} = E_{Liq} + E_{Sol} \quad (51)$$

where  $E_{Liq}$  and  $E_{Sol}$  represent the (reduced) PCM energies in the liquid and the solid phases, respectively, given by:

$$E_{liq} = \iint_{D_L} \rho_L C_{pL} \delta\theta_L dz dy; \quad E_{Sol} = \iint_{D_S} \rho_S C_{pS} \delta\theta_S dz dy \quad (52)$$

where  $\delta\theta_L$  and  $\delta\theta_S$  represent the difference between the mean temperature at the current instant  $t$  and the mean temperature at the initial instant  $t=0$  in the liquid and the solid domains, respectively:

$$\delta\theta_L = (\theta_m)_L(t) - (\theta_m)_L(0); \quad \delta\theta_S = (\theta_m)_S(t) - (\theta_m)_S(0) \quad (53)$$

Note that a mean temperature  $\theta_m(t)$  in any domain  $D$  is given by:

$$\theta_m(t) = \frac{\iint_D \theta(y, z, t) dydz}{\iint_D dydz} \quad (54)$$

To quantify the dynamics in the liquid domain, we define the reduced kinetic energy in the liquid phase by the Euclidian norm of the velocity vector  $\vec{V}$  on the collocation points:

$$E_{kin} = \left\| \vec{V} \right\| = \sqrt{\sum_{i=0}^{N_x} \sum_{j=0}^{N_r} (u^2(x_i, r_j) + v^2(x_i, r_j))} \quad (55)$$

Figure 8 shows its temporal evolution and confirms the existence of the critical time indicating the transition from conductive to convective phase. We see in Figure 8 that kinetic energy and mean temperature behaviours in the liquid phase are of course in opposite evolution: when the kinetic energy increases, particularly at  $t = t_{crit}$ , the mean temperature decreases in the fluid, and conversely.

We also clearly notice a second and sudden short gap of the both kinetic energy and mean liquid temperature time-evolution in the convective regime, characterized by short-lived fluctuations of high amplitudes, starting at  $t \approx 1,100$  s and stopping at  $t = t_{end} \approx 1,190$  s. Past this melting process time-end  $t = t_{end}$ , kinetic energy and mean liquid temperature keep a constant value. This second critical time  $t = t_{contact} \approx 1,100$  s

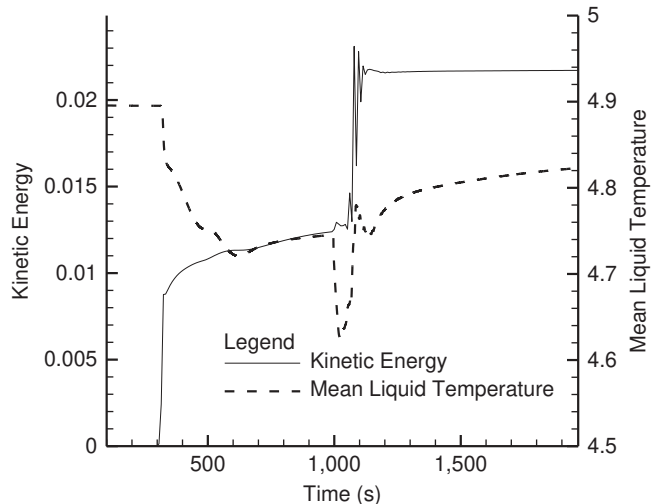


**Figure 8.** Temporal evolution of the kinetic energy and the liquid mean temperature

is due to the existence of the first points achieving their melting process and then coming in contact with the insulated top surface cell.

Figure 9 shows the temporal evolution of the liquid fraction, the total energy and the mean temperature on the whole PCM cell. The liquid fraction behaviour allows us to verify the global evolution of the heat transfer between the two phases: solid and liquid. The general evolution of this curve is also classical. We notice that in the purely conductive phase, the liquid fraction evolves as  $t^\alpha$  law, with  $\alpha \approx 0.53$  here. As for Equation (74) (see also Gong and Mujumdar, 1998), the exact value of  $\alpha$  is:  $\alpha = 0.5$ . The slight difference between the exact value and the value provided by this model is probably due to the hypothesis of the presence of a few quantity of liquid at the initial instant  $t = 0$  in our model (Section 9.1). Past the time  $t = t_{crit} \approx 330$  s, in the convective phase, this evolution remains almost linear. The total energy and the PCM mean temperature curves are similar to the liquid fraction evolution, except at time  $t \approx 900$  s where these curves begin to increase.

To understand the thermal fluid behaviour in relation to the PCM melting process, Figure 10 presents the temporal evolution of the unsteady temperature at the control points, indicated in Figure 3. We observe that this evolution is uniform in the conductive phase. A sudden increase or decrease happens at the critical time  $t = t_{crit} \approx 330$  s, depending on the position of the control point. Past this moment and after a transient stage characterised by some oscillations closed to the critical time, the fluid temperature temporal evolution at all points seems almost stationary, except during the second slight and short disturbance occurred at  $t = t_{contact} \approx 1,100$  s due to the first points achieving their melting process and then coming in contact with the insulated top surface cell, as mentioned above. Although the five control points are geometrically symmetrical in relation to the central point 3, Figure 10 shows that their thermal and dynamic behaviours are not symmetrical.

*9.2.4 The end of the melting process.* The end of the melting process proceeds as follows: after the disruptions generated by the transition from conductive phase to convective phase and as long as the liquid domain has not yet reached its maximal height, the number of vortexes in the liquid domain remains stable (Figure 11).

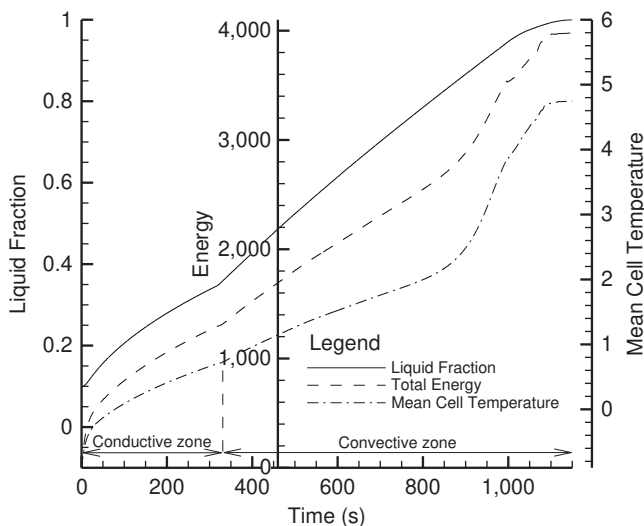
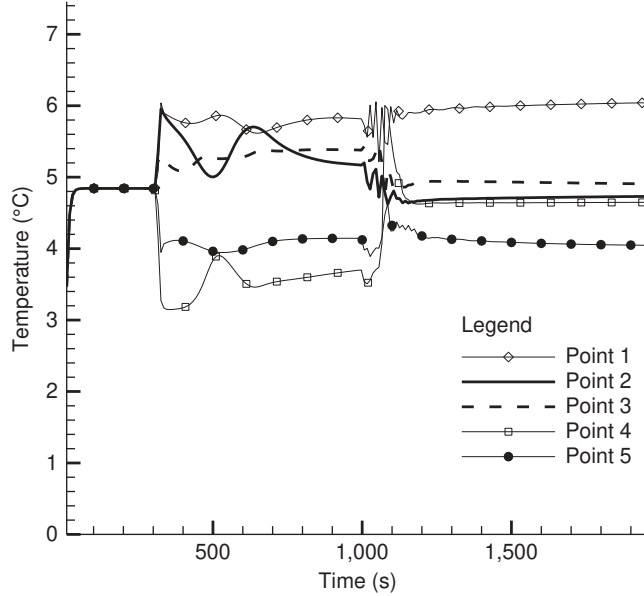


**Figure 9.** Temporal evolution of the liquid fraction, the total energy and the mean cell temperature

**Figure 10.** Temporal evolution of the control points temperature



However, gradually as the solid layers complete their melting process, the number of vortexes decreases in time. Some adjacent vortexes merge together to form a single vortex. This process continues until total solid mass melting. In the present case, it remains only three vortexes at the end of this melting process. When all the solid mass has melted (Figure 12), the dynamic and thermal fields in the liquid domain tend progressively towards a steady state.

### 9.3 Study on numerical results accuracy

To ensure the accuracy of our results from the numerical point of view, we try several orders of truncature in the Chebyshev basis developments and different time steps (Batchi, 2005). Except express mention of the opposite, all this survey concerns the liquid domain. First, we give some definitions relative to Chebyshev standard spaces.

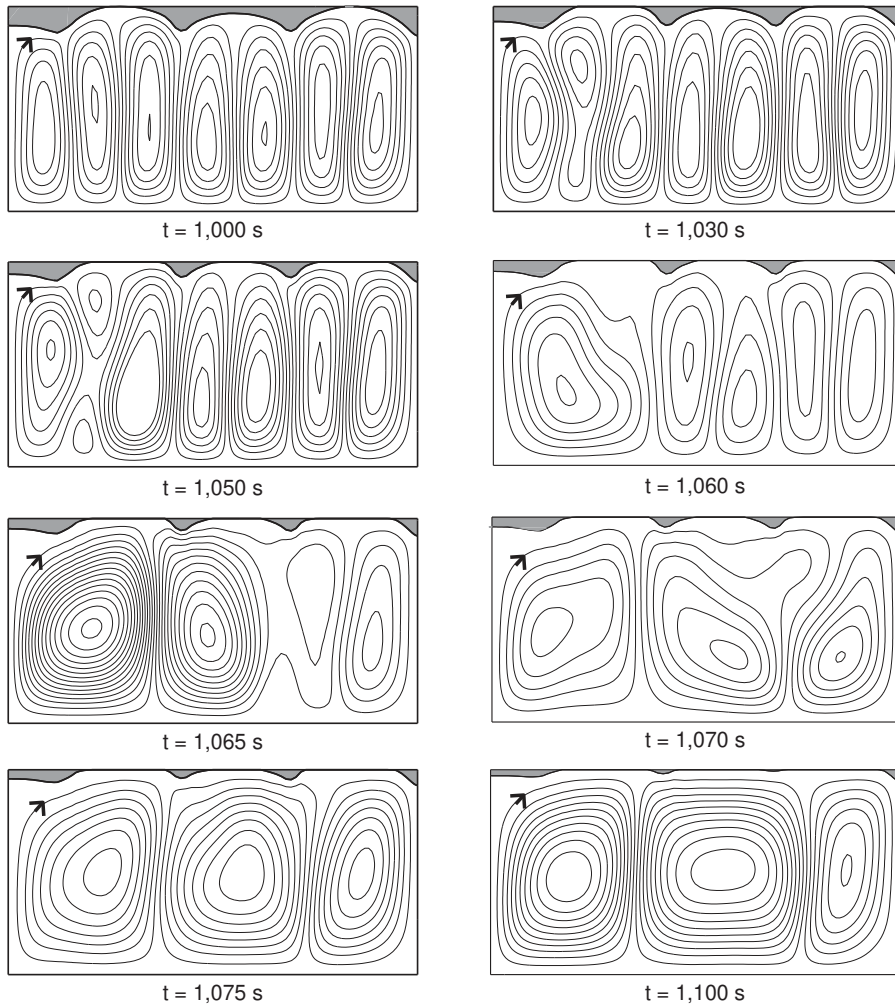
*9.3.1 Chebyshev standard spaces and truncature errors definitions.* For two given polynomial functions  $\psi(x, r)$  and  $\phi(x, r)$ , one defines their Chebyshev scalar product by:

$$\langle \psi, \phi \rangle = \frac{4}{\pi^2} \iint_{\Delta} \psi(x, r) \phi(x, r) \frac{1}{\sqrt{1-x^2}} \cdot \frac{1}{\sqrt{1-r^2}} dx dr \quad (56)$$

where  $\Delta$  is the square:  $\Delta = [-1, 1] \times [-1, 1]$ .

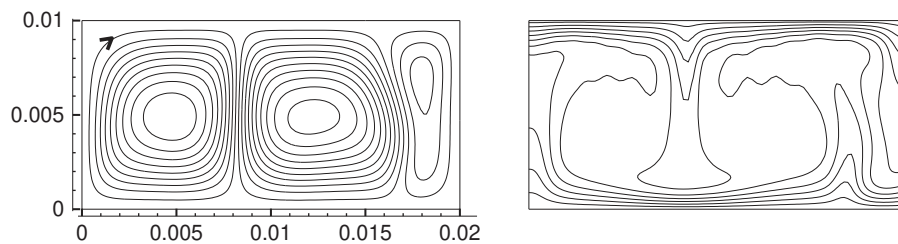
For our discretized unsteady stream functions, we have:

$$\begin{aligned} \psi(x, r, t) &= \sum_{k=0}^{N_x} \sum_{l=0}^{N_r} \psi_{kl}(t) P_l(r) Q_k(x) \text{ and} \\ \phi(x, r, t) &= \sum_{i=0}^{N_x} \sum_{j=0}^{N_r} \phi_{ij}(t) P_j(r) Q_i(x) \end{aligned} \quad (57)$$



**Notes:** For  $t \leq 1,065$  s:  $N_\psi = 12$ ,  $\Psi_{min} = -1.10^{-6}$ ,  $\Psi_{max} = 1.10^{-6}$ ; for  $t \geq 1,070$  s:  $N_\psi = 30$ ,  $\Psi_{min} = -5.10^{-6}$ ,  $\Psi_{max} = 5.10^{-6}$

**Figure 11.**  
Temporal evolution  
of streamlines showing  
the end of the  
PCM melting



**Notes:**  $N_\psi = 20$ ,  $\Psi_{min} = -4.10^{-6}$ ,  $\Psi_{max} = 4.10^{-6}$ ;  $N_\theta = 10$ ,  $\theta_{min} = 0^\circ\text{C}$ ,  $\theta_{max} = 9^\circ\text{C}$

**Figure 12.**  
Streamlines and  
corresponding  
isotherms past the  
total PCM melting

Then, their scalar product (56) becomes:

$$\begin{aligned}\langle \psi, \phi \rangle &= \sum_{k=0}^{N_x} \sum_{l=0}^{N_r} \sum_{i=0}^{N_x} \sum_{j=0}^{N_r} \psi_{kl}(t) \phi_{ij}(t) \langle P_l, P_j \rangle \langle Q_k, Q_i \rangle \\ &= \sum_{i=0}^{N_x} \sum_{j=0}^{N_r} \left\{ \phi_{ij}(t) \left[ \sum_{k=0}^{N_x} \sum_{l=0}^{N_r} \psi_{kl}(t) \langle P_l, P_j \rangle \langle Q_k, Q_i \rangle \right] \right\}\end{aligned}\quad (58)$$

Let us write:

$$\Psi_i^j(t) = \langle \psi, P_j Q_i \rangle = \sum_{k=0}^{N_x} \sum_{l=0}^{N_r} \psi_{kl}(t) \langle P_l, P_j \rangle \langle Q_k, Q_i \rangle \quad (59)$$

Then, the Chebyshev scalar product in the space of discretized stream functions becomes:

$$\langle \psi, \phi \rangle = \sum_{i=0}^{N_x} \sum_{j=0}^{N_r} \phi_{ij}(t) \Psi_i^j(t) \quad (60)$$

The Chebyshev norm of the stream function  $\psi$  is given by:

$$\|\psi\| = \sqrt{\langle \psi, \psi \rangle} \quad (61)$$

This analyse is also available for the temperature field, by substituting the Chebyshev polynomials  $P$  and  $Q$  by  $p$  and  $q$ , respectively.

For reasons of simplicity, our numerical errors studies will concern only the temperature field. The same analysis applied to the stream function field lead to identical conclusions.

The different truncature errors are linked to three parameters: the polynomial developments truncature orders  $N_x$  and  $N_r$  and the time-step  $\Delta t$ . For numerical tests, we define three sets: the truncature order  $N_x$  (respectively  $N_r$ ) is chosen in a set of increasing integer values  $S_{N_x}$  (respectively  $S_{N_r}$ ) and the time-step  $\Delta t$  is chosen in a set of decreasing real values  $S_{\Delta t}$  (given in seconds). Because of the difficulty to represent the three parameters varying simultaneously, we have chosen to fix two parameters and to let the third parameter free. So, we consider three kinds of numerical errors:

Numerical study according to  $N_x$  parameter.  $\Delta t \in S_{\Delta t}$  and  $N_r \in S_{N_r}$  being fixed, let  $E_{N_x}(N_r, \Delta t)$  be the time-dependent truncature error calculated between two consecutive temperature fields, when  $N_x$  increases in  $S_{N_x}$ . To define the expression of  $E_{N_x}(N_r, \Delta t)$ , we rewrite differently the expression of the temperature field  $\theta$  given by Equation (33). Because the temperature Chebyshev coefficients  $\theta_{kl}$  depend also on the time-step  $\Delta t$ , we write:

$$\theta(x, r, \Delta t) = \theta_{N_x}^{N_r}(\Delta t) = \sum_{k=0}^{N_x} \sum_{l=0}^{N_r} \theta_{kl}(\Delta t) q_k(x) p_l(r) \quad (62)$$

Then,  $E_{N_x}(N_r, \Delta t)$  is defined by:

$$E_{N_x}(N_r, \Delta t) = \frac{\left\| \theta_{N_x}^{N_r}(\Delta t) - \theta_{N_x}^{N_r}(\Delta t) \right\|}{\left\| \theta_{ref} \right\|} \quad (63)$$

where  $N_x^-$  represents the previous value of  $N_x$  in the set  $S_{N_x}$ . For example, if we choose  $S_{N_x} = \{10, 15, 20\}$ , then the couple  $(N_x^-, N_x)$  can take the values (10, 15) and (15, 20).  $\theta_{ref}$  is a reference temperature, chosen here equal to the imposed bottom cell temperature.

For a cell whose bottom wall is subjected to a uniform given heat flux, one can take  $T_{ref}$  equal to the time-averaged expression of the mean bottom cell temperature  $\theta_m(t)$  given by Equation (69).

Numerical study according to  $N_r$  parameter. In the same manner as the previous study,  $\Delta t \in S_{\Delta t}$  and  $N_x \in S_{N_x}$  being fixed, we study the behaviour of the numerical error  $E_{N_r}(N_x, \Delta t)$  defined by:

$$E_{N_r}(N_x, \Delta t) = \frac{\left\| \theta_{N_x}^{N_r^-}(\Delta t) - \theta_{N_x}^{N_r}(\Delta t) \right\|}{\left\| \theta_{ref} \right\|} \quad (64)$$

where  $N_r^-$  represents the previous value of  $N_r$  in the set  $S_{N_r}$ .

Numerical study according to  $\Delta t$  parameter. To study the accuracy of the numerical solution according to the time-step parameter, we fix  $N_x \in S_{N_x}$  and  $N_r \in S_{N_r}$ , and we study the behaviour of the numerical error  $E_{\Delta t}(N_x, N_r)$ , with:

$$E_{\Delta t}(N_x, N_r) = \frac{\left\| \theta_{N_x}^{N_r}(\Delta t^-) - \theta_{N_x}^{N_r}(\Delta t) \right\|}{\left\| \theta_{ref} \right\|} \quad (65)$$

where  $\Delta t^-$  represents the previous value of  $\Delta t$  in the set  $S_{\Delta t}$ .

We give below the main truncature orders and the different time-steps that we tested:

$$S_{N_x} = \{10, 15, 20, 30, 32, 34, 36, 38, 40\} \quad (66)$$

$$S_{N_r} = \{10, 12, 14, 16, 18\} \quad (67)$$

$$S_{\Delta t} = \{1.6s, 0.8s, 0.4s, 0.2s, 0.1s, 0.05s\} \quad (68)$$

The numerical errors  $E_{N_r}(N_x, \Delta t)$ ,  $E_{N_x}(N_r, \Delta t)$  and  $E_{\Delta t}(N_x, N_r)$  are time-dependent. So, it is necessary to fix an interval of time  $[0, t_{comp}]$  for comparisons. Let us define  $t_{fusion}$  as the necessary time to achieve the PCM melting process. On the one hand,  $t_{comp}$  must verify:  $t_{comp} \leq t_{fusion}$ . On the other hand,  $t_{comp}$  must be chosen far from the critical time  $t_{crit}$  representing the beginning of the convective phase. Our results give:  $t_{crit} \approx 330$  s and  $t_{fusion} \approx 1,194$  s. In view to reduce computational time and because it is not necessary to have  $t_{comp} = t_{fusion}$ , we took approximately:

$$t_{comp} \approx 800s. \text{ So : } \frac{t_{comp}}{t_{fusion}} \approx 67\% \quad (69)$$

Moreover, to have a general overview of any given truncature error  $E$ , it is useful sometimes to define its averaged expression on the interval  $[0, t_{comb}]$  as follows:

$$\bar{E} = \frac{1}{t_{comb}} \int_0^{t_{comb}} E dt \quad (70)$$

where  $E$  represents  $E_{N_x}(N_r, \Delta t)$  or  $E_{N_r}(N_x, \Delta t)$  or  $E_{\Delta t}(N_x, N_r)$ .

We can now study the behaviour of our computed solutions when the main numerical parameters  $N_x$ ,  $N_r$  and  $\Delta t$  vary.

*9.3.2 Numerical study according to  $N_x$  parameter.* Let us fix  $\Delta t = 0.1$  s for the time-step and  $N_r = 18$  for the truncature order in the vertical direction. Our aim is to determine approximately one or several values of  $N_x$  assuring the best accuracy and the best convergence of numerical results, i.e. for which  $E_{N_x}$  or  $\bar{E}_{N_x}$  is minimal.

In Figure 13, when  $N_x < 30$ , we observe first that the truncature errors  $E_{N_x}(N_r = 18, \Delta t = 0.1$  s)(or more shortly  $E_{N_x}$ ) depend mainly on the parameter  $N_x$ . Second, we note that these curves are quite stable in the conductive phase, in which the truncature errors  $E_{N_x}$  are negligible, about 1 per cent, but oscillate highly past the critical time  $t_{crit}$ . The first curve with weak fluctuations occurs at  $N_x = 30$ . Therefore, to ensure the stability and the convergence of numerical results for  $\Delta t = 0.1$  s and  $N_r = 18$ , we have to increase  $N_x$  beyond 30.

The aim of Figure 14 is to explore more finely the region  $30 \leq N_x \leq 40$ . The numerical results convergence is clearly highlighted in this figure: the critical time  $t_{crit}$  does not depend anymore on  $N_x$ ; the different curves  $E_{N_x}$  are almost identical when  $N_x > 32$ . Therefore, it is suitable to choice  $N_x = 40$ . It is important to note that the critical time  $t_{crit}$  representing the transition from conductive phase to convective region is independent of the  $N_r$  parameter.

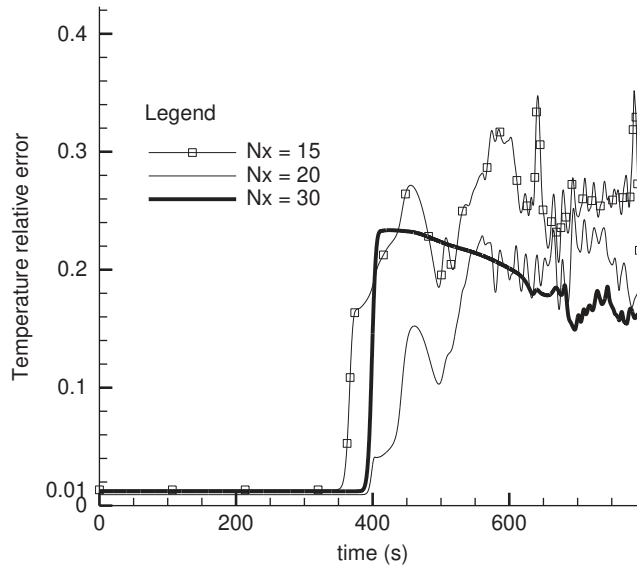
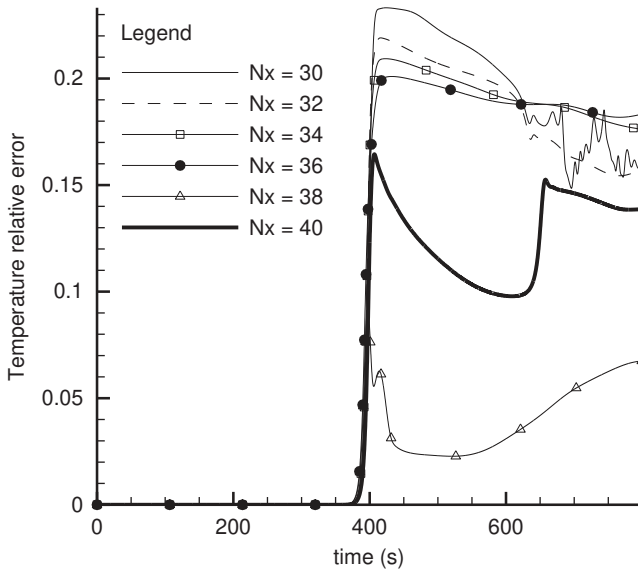


Figure 13. Temporal evolution of the truncature errors  $E_{N_x}(N_r = 18; \Delta t = 0.1$  s) with  $N_x < 30$



**Figure 14.** Temporal evolution of the truncature errors  $E_{N_x}(N_r = 18, \Delta t = 0.1 \text{ s})$  with  $30 \leq N_x \leq 40$

**9.3.3 Numerical study according to  $N_r$  parameter.** With reference to the previous study, our aim is to verify that, for  $\Delta t = 0.1 \text{ s}$  and  $N_x = 40$ , a suitable order of Chebyshev polynomials developments according to the axis  $r$  is  $N_r = 18$ , for which a good accuracy of numerical results, represented by the truncature error  $E_{N_x}$ , is assumed.

But, unlike our hypothesis, we observe in Figure 15 that the truncature errors  $E_{N_x}$  increase with the values of  $N_r$ , included between 12 and 14, so that the best choice of  $N_r$  seems to be  $N_r = 12$ . This inconsistent result leads us to refine our analysis. Parametric studies according to  $N_r$  of dynamic and thermal liquid phase behaviours (Figures 16 and 17) show that  $N_r = 12$  or  $N_r = 14$  are not suitable truncature orders.

Indeed, these weak values are not sufficiently high to take into account the second sudden increase of the thermal energy  $\frac{\|\theta\|}{\|\theta_{ref}\|}$  (Figure 16) or the kinetic energy  $E_{kin}$  (Figure 17), located at  $t = 630 \text{ s}$ . Consequently, a good numerical approximation of dynamic and thermal fields is clearly obtained for  $N_r > 14$ . In fact, Figure 15 shows that optimal accuracy is obtained for  $N_r = 18$ . One can notice that the transition time  $t_{crit}$  from conductive phase to convective region does not depend on  $N_r$  parameter.

**9.3.4 Numerical study according to time-step parameter.** Finally, we have to study the truncature errors  $E_{\Delta t}(N_x = 40, N_r = 18)$  for different time steps  $\Delta t$  in the set  $S_{\Delta t}$ . We recall that our aim is to find approximately one or several values of  $\Delta t$  leading to the best numerical results accuracy, i.e. for which  $E_{\Delta t}(N_x = 40, N_r = 18)$  is minimal.

As for  $N_x$  parameter study, we observe in Figure 18 first that the truncature errors  $E_{\Delta t}$  depend strongly on the parameter  $\Delta t$ , and second, truncature errors decrease with  $\Delta t$ , until  $\Delta t = 0.1 \text{ s}$ . We note also the stability of  $E_{\Delta t}$  in the conductive phase, where its values are negligible, about 1 per cent. We deduce from this figure that the time step optimal value is obtained about  $\Delta t \approx 0.1 \text{ s}$ . This result is confirmed by the study of the time-averaged truncature errors  $\bar{E}_{\Delta t}$  (Figure 19). This study shows once again that the transition time  $t_{crit}$  from conductive phase to convective region is not affected by the time-step parameter.

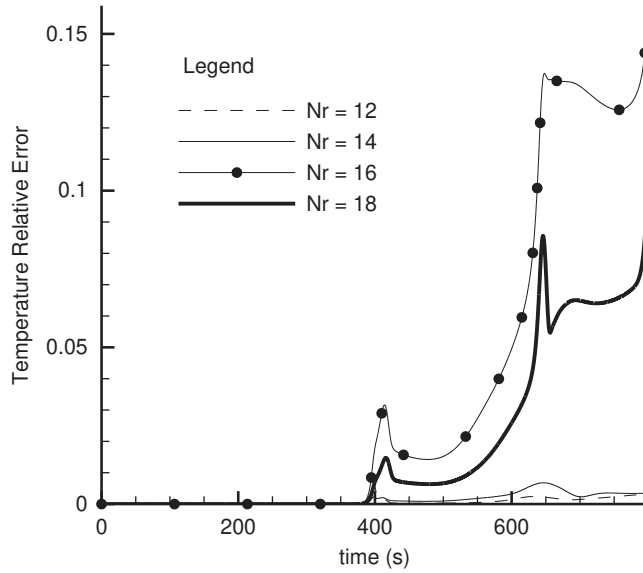


**Figure 15.**  
Temporal evolution of  
the truncature errors  
 $E_{N_r}$  ( $N_x = 40$ ,  $\Delta t = 0.01$  s)

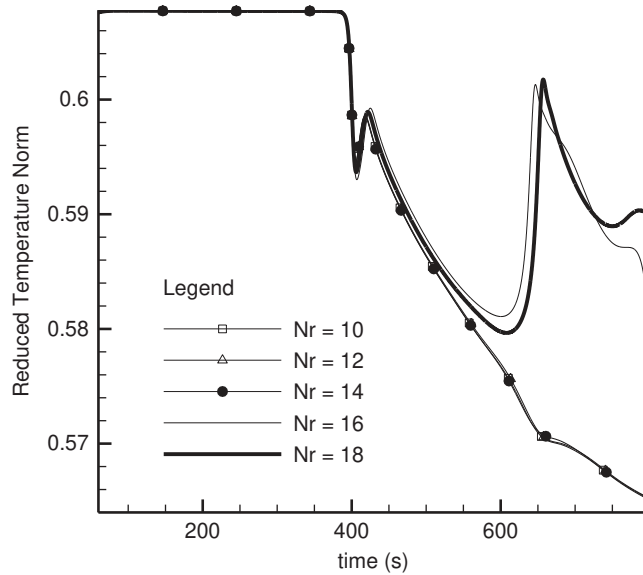


**Figure 16.**  
Temporal evolution of  
the reduced temperature  
norm  $\frac{\|\theta\|}{\|\theta_{ref}\|}$

In conclusion, to assume optimal numerical accuracy, we have selected for this problem the following numerical parameters:  $N_x = 40$ ,  $N_r = 18$  and  $\Delta t = 0.1$  s.

#### 9.4 Validation tests

In view to test and validate the numerical accuracy of the present modelling of a PCM melting process heated from below using spectral collocation methods, the numerical procedure is submitted to the three tests described in the following analysis.

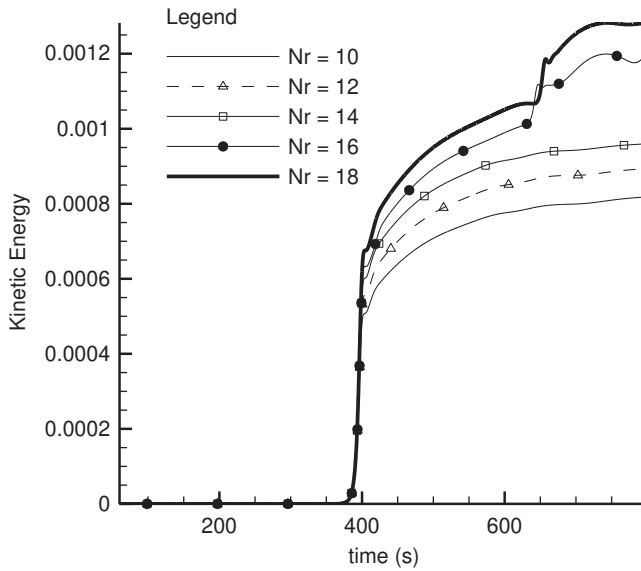


**Figure 17.**  
Temporal evolution  
of the kinetic energy

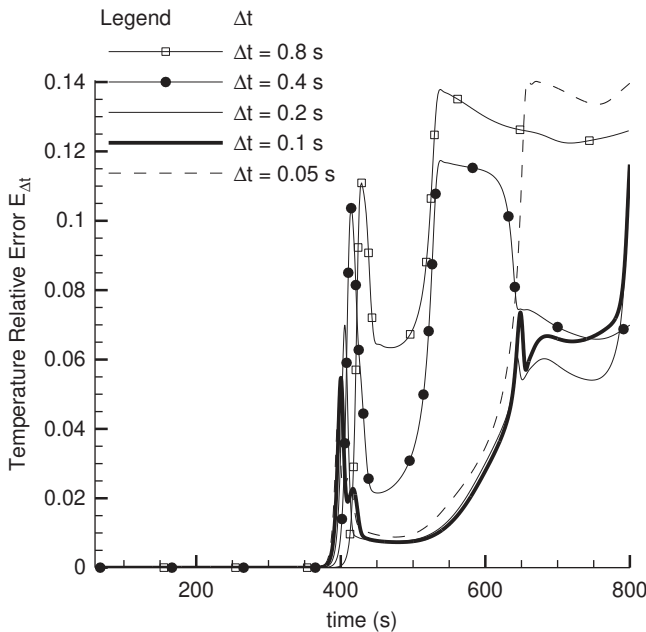
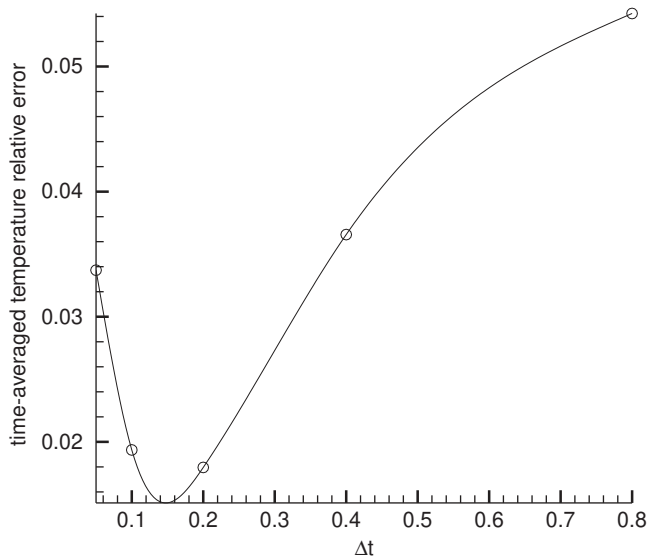


**Figure 18.**  
Temporal evolution of  
the truncature errors  
 $E_{\Delta t}(N_x = 40, N_r = 18)$

These problems have been chosen because they are closed to the present study. The case of particular PCM materials like some liquid metals such as the pure gallium (see e.g. Fteïti and Nasrallah, 2004) will be the subject of a second survey because their temporal physical behaviours require some particular precautions in the numerical simulation procedures.

**Figure 19.**  
Time-averaged  
relative error  
 $\bar{E}_\Delta(N_x = 40, N_r = 18)$



*9.4.1 Test 1: the classical Stefan problem.* The numerical accuracy of the temporal evolution of the interface solid/liquid algorithm used in this paper is tested on to the classical Stefan problem (Rubinstein, 1971), proposed by Wintruff *et al.* (2001). It consists to study the temporal evolution of the solid/liquid PCM boundary in a 1D half-space cell  $z \geq 0$ . Initially, the cell is filled with a liquid at a constant temperature  $\theta_2 > \theta_M$ . At time  $t = 0$  the boundary  $z = 0$  is cooled to a temperature  $\theta_1 < \theta_M$ . The solid phase domain increases with time. According to general hypothesis and physical PCM properties discussed in Wintruff *et al.* (2001) work, this problem is governed by the unsteady 1D heat conduction equations in the solid and liquid phases, respectively:

$$\rho_S C_{P_S} \frac{\partial \theta_S}{\partial t} = \lambda_S \frac{\partial^2 \theta_S}{\partial z^2} \quad (71)$$

$$\rho_L C_{P_L} \frac{\partial \theta_L}{\partial t} = \lambda_L \frac{\partial^2 \theta_L}{\partial z^2} \quad (72)$$

In both solid and liquid phases, all physical parameters  $\rho$ ,  $\lambda$  and  $C_P$  are assumed to be constant in space and time. The interface solid/liquid (subscript  $I$ ) is at a constant temperature  $\theta_M$  and its position  $z_I$  is governed by the equation:

$$\rho_S L a \frac{\partial z_I}{\partial t} = \lambda_L \left( \frac{\partial \theta_L}{\partial z} \right)_I - \lambda_S \left( \frac{\partial \theta_S}{\partial z} \right)_I \quad (73)$$

Analytical solution of this problem is given by:

$$z_I(t) = 2\zeta \sqrt{a_S t} \quad (74)$$

where  $\xi$  is the solution of the non-linear equation:

$$\frac{e^{-\xi^2}}{\text{erf}(\xi)} - \frac{\lambda_S \sqrt{a_S}}{\lambda_L \sqrt{a_L}} \frac{(\theta_2 - \theta_M) e^{-a_S \xi^2 / a_L}}{(\theta_M - \theta_1) \text{erfc}(\xi \sqrt{a_S / a_L})} = \frac{\xi L a \sqrt{\pi}}{C_{P_S} (\theta_M - \theta_1)} \quad (75)$$

The unsteady temperature field is given by:

$$\theta(z, t) = \begin{cases} \theta_1 + \frac{\theta_M - \theta_1}{\text{erf}(\xi)} \text{erf}\left(\frac{z}{2\sqrt{a_S t}}\right) & \text{if } z < z_I \\ \theta_M & \text{if } z = z_I \\ \theta_2 - \frac{\theta_2 - \theta_M}{\text{erf}(\xi \sqrt{a_S / a_L})} \text{erfc}\left(\frac{z}{2\sqrt{a_L t}}\right) & \text{if } z > z_I \end{cases} \quad (76)$$

We solved numerically this problem in a 2D cell with an aspect ratio  $A = 0.1$ , using spectral-collocation and Crank-Nicolson methods described in Sections 6 and 7, with the same physical PCM parameters as in Wintruff, summarized in Table I.

Results and discussion. Let us consider a fixed point  $z_P$  located at the fixed position  $z_P = 0.1 \times L_z$ , where  $L_z$  is the total length of the cell. Figure 20(a) and (b) show comparisons between analytical and numerical solutions of the temporal evolution of the solid/liquid interface  $z_I$  and the temperature of the point  $z_P$  respectively.

In Figure 21, we can follow the numerical versus analytical solutions of the temperature profiles temporal evolutions along the cell axis at fixed times.

Aspect ratio	$A = 0.1$	<b>Table I.</b> Physical properties and non-dimensional parameters used in the simulation of a two-phase Stefan problem
Melting temperature	$\theta_M = 0^\circ\text{C}$	
Cooling temperature	$\theta_1 = -10^\circ\text{C}$	
Initial temperature	$\theta = \theta_2 = 2^\circ\text{C}$	
Mass density	$\rho_S = \rho_L = 1 \text{ kg/m}^3$	
Heat conductivity	$\lambda_S = \lambda_L = 2 \text{ W/mK}$	
Specific heat	$C_{P_S} = C_{P_L} = 2.5 \times 10^6 \text{ J/kgK}$	
Latent heat	$L a = 1 \times 10^8 \text{ J/kg}$	
Stefan number	$Ste = 0.25$	

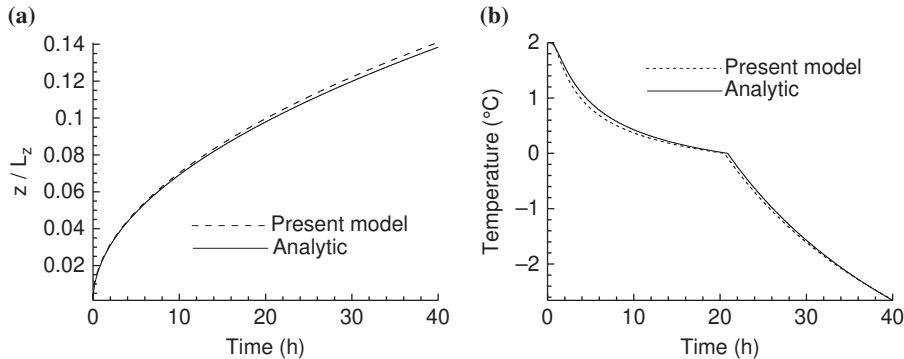


**Figure 20.**  
 Comparison between analytical and numerical solutions of the temporal evolution of the (a) solid/liquid interface  $z_I$ , (b) fixed point temperature  $z_P = 0.1 \times L_z$

All these results show an excellent agreement between analytical and numerical solutions. The maximum error is about 0.7 per cent for the front position and 0.5 per cent for the temperature profiles.

*9.4.2 Test 2: the paraffin melting in Gong study.* In the second problem used to test the accuracy of our numerical procedures, we compare numerical results obtained by Gong and Mujumdar numerical work (Gong and Mujumdar, 1998) and the present model. It concerns the melting of a PCM (paraffin) in a rectangular cell heated from below. The top and the two vertical walls are assumed to be adiabatic. The used physical parameters are in Table II.

Results and discussion. In the conductive zone ( $t < 200$  s), our results are similar to those obtained by Gong. However, in the convective regime (Figure 22), the present model provides the same results as Gong model, but at time sections slightly shifted. For example, streamlines and isotherms obtained by Gong for  $t = 342.5$  s are identical to those obtained by the present model at time  $t \approx 420$  s (Figure 22(c) and (C) for streamlines, Figure 22(f) and (F) for isotherms). The temporal evolution of the dimensionless heat flux distribution along the heated wall obtained by the two models is almost identical, as shown in Figure 23.

*9.4.3 Test 3: an experimental Benchmark problem.* To achieve the present model validation, we consider the natural PCM melting, heated from below, studied experimentally by Dietsche and Müller (1985) and numerically by Wintruff *et al.* (2001). The experimental PCM cell is a 2D rectangular box with an aspect ratio larger than 1:10. Due to this parameter and other physical data, as mentioned by Winturff, “a numerical simulation that exactly reproduces the history of the transient experiments was not possible”. So, numerical study of this problem is only a first approach of the physical situation. However, we can carry out some significant conclusions dealing with experiments results. The used PCM is the cyclohexane ( $Pr = 18$ ) in a cell whose bottom wall is heated at constant temperature  $\theta = \theta_W = 8.5^\circ\text{C}$  while the top wall is cooled at a constant temperature  $\theta = \theta_{top} = 5.46^\circ\text{C}$ . The two vertical walls are

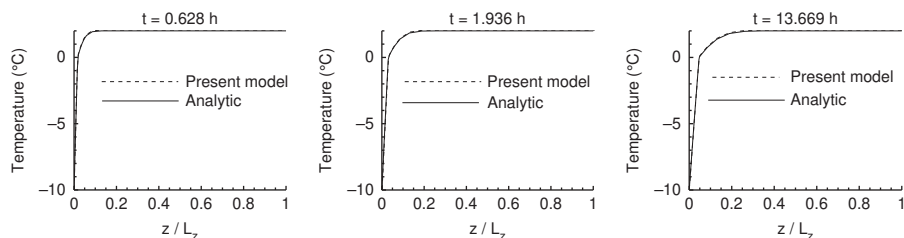
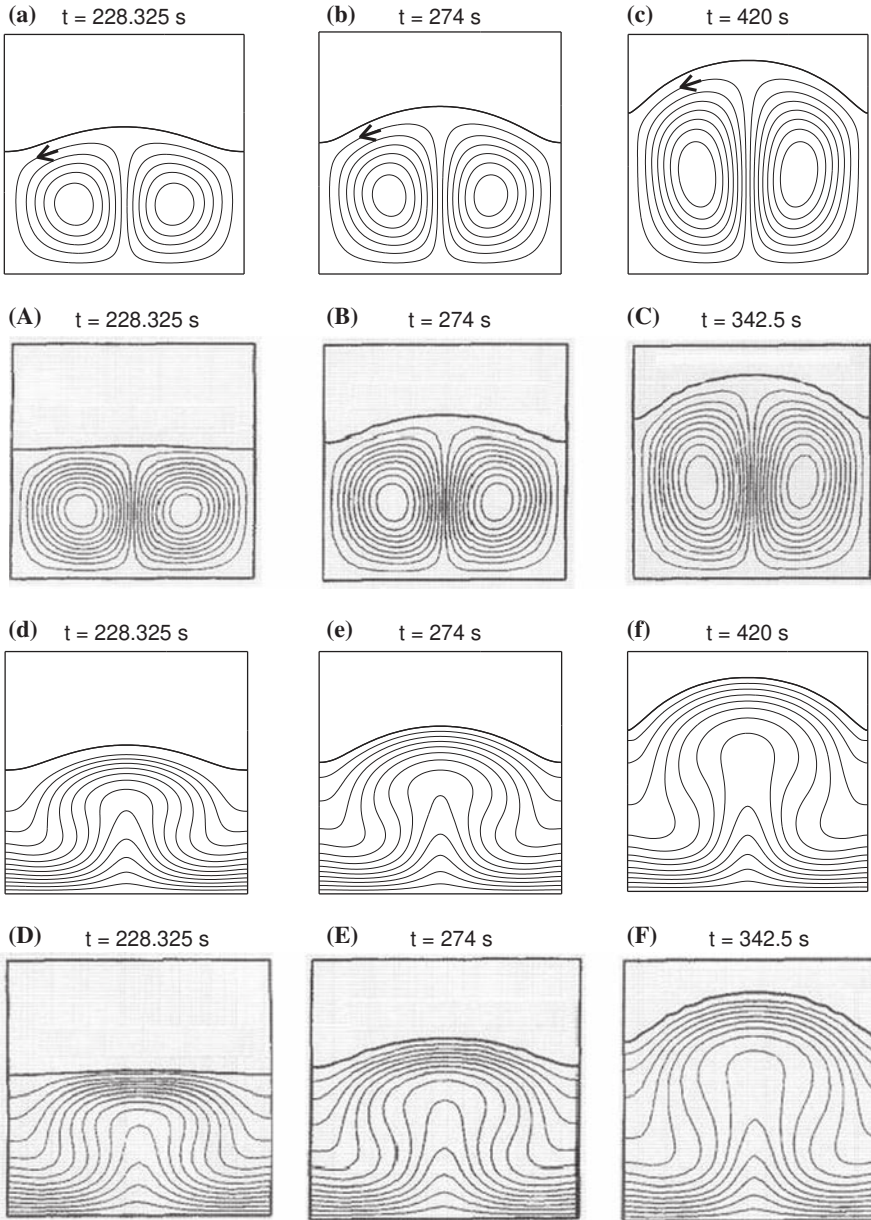


**Figure 21.** Comparisons between analytical and numerical temperature profiles at fixed times

**Table II.** Physical properties and non-dimensional parameters used in the simulation of the paraffin melting in Gong study

Aspect ratio	$A = 1$
Raleigh number	$Ra = 2.844 \times 10^6$
Prandtl number	$Pr = 46.1$
Stefan number	$Ste = 0.138$
Bottom temperature	$\theta_W = 29.96^\circ\text{C}$
Melting temperature	$\theta_M = 17^\circ\text{C}$
Initial temperature	$\theta = 16.7^\circ\text{C}$
Ratio of solid/liquid specific heat	$C_{P_S}/C_{P_L} = 0.964$
Ratio of solid/liquid conductivity	$\lambda_S/\lambda_L = 2.419$



**Notes:** Small letters: present model; capital letters: Gong model. Streamlines:  $N_\psi = 14$ ,  $\Psi_{min} = -4.10^{-7}$ ,  $\Psi_{max} = 4.10^{-7}$ ; Isotherms:  $N_\theta = 12$ ,  $\theta_{min} = 19^\circ\text{C}$ ,  $\theta_{max} = 29^\circ\text{C}$

**Figure 22.** Streamlines (a), (b), (c), (A), (B), (C) and corresponding isotherms at different time steps

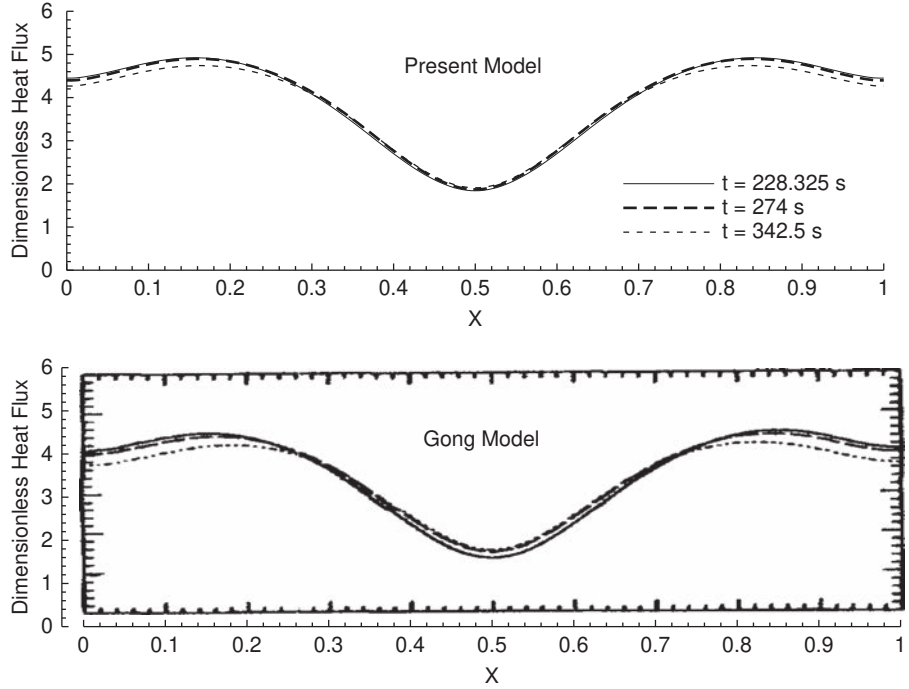


**Figure 23.** Local dimensionless heat flux distribution along the heated surface at different time steps

assumed to be adiabatic. The cell aspect ratio varies from 1:4 to 1:8. The aim of the experimental work is to characterize the flow structure in steady state regime. The used physical parameters are summarized in Table III.

Note that Bi is the Biot number, defined by:

$$Bi = \frac{\lambda_S \theta_M - \theta_{top}}{\lambda_L \theta_W - \theta_M} \quad (77)$$

Results and discussion. The obtained results are qualitatively in agreement with the general expected results: multicellular flow in the convective region, modal flow structure in the neigh borrows of vertical walls, steady state flow obtained before the total PCM melting, etc. According to the liquid fraction temporal evolution

<b>Table III.</b>		
Physical properties and non-dimensional parameters used in the simulation of an experimental Benchmark problem	Aspect ratio	$A = 1:4$ and $A = 1:8$
	Raleigh number	$Ra = 10,700$
	Prandtl number	$Pr = 18$
	Biot number	$Bi = 1.386$
	Top temperature	$\theta_{top} = 5.46^\circ\text{C}$
	Bottom temperature	$\theta_W = 8.5^\circ\text{C}$
	Melting temperature	$\theta_M = 6.85^\circ\text{C}$
	Initial temperature	$\theta = 6.7^\circ\text{C}$
	Ratio of solid/liquid specific heat	$C_{Ps}/C_{PL} = 0.96$
	Ratio of solid/liquid conductivity	$\lambda_S/\lambda_L = 1.02$

(Figure 25(d)), the steady state regime seems to be reached. But the local bimodal flow structure is not detected by the present model. Indeed, Figures 24 and 25 show that the bimodal flow structure phenomenon depends on the PCM cell aspect ratio and appears far from the vertical walls because of the presence of boundary conditions. For this reason, to simulate correctly this physical flow structure, the numerical accuracy of the used scheme must be excellent in the cell central region. Unfortunately, the Gauss-Lobatto spectral method is not adapted to this situation, except if we increase greatly the polynomial Chebyshev degrees in the axis direction, and consequently the CPU time calculations. Moreover, according to Wintruff discussion, the numerical solution in the steady state regime depends on:

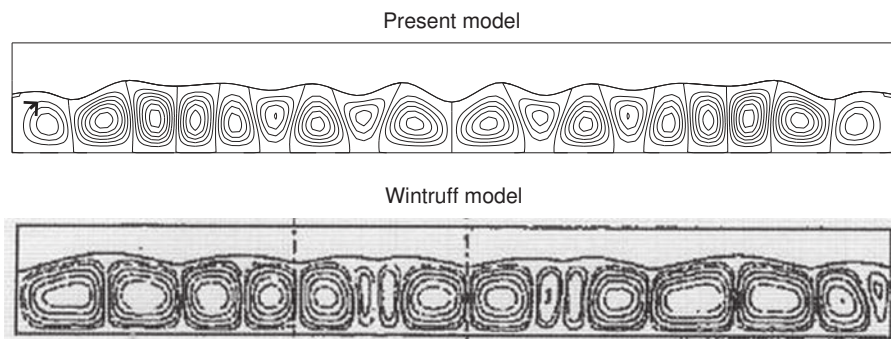
- the initial solution used;
- the method used to increase the Raleigh number;
- the aspect ratio of the PCM domain; etc.

Wintruff conclusion is: “A large variety of patterns that seem to be stationary and stable during the time scale resolved by the numerical simulation can occur”. The present work agrees this analysis.

In a final conclusion of all these comparisons, our numerical model is validated by these Benchmark exercises and its accuracy is in good agreement with the numerical methods used by the authors like Gong and Mujumdar (1998) or Wintruff *et al.* (2001).

## 10. Conclusions

In this paper, numerical studies have been carried out on a modelling of melting process in a cell containing a PCM. Thus, the study emphasizes on the heat and mass transfer modifications. During the melting time process, the material in the PCM cell is in one or two phases, solid/liquid. The interface separating the two phases is a critical unknown of the problem. The physical model and the numerical method chosen to study the both conductive and convective liquid phase of the PCM on the one hand and the time-evolution of its liquid-solid interface on the other hand, have given entirely satisfactory, in accordance with the almost well-known literature surveys. The results have clearly shown the transition from a multicellular regime with several vortexes into a multicellular regime with a few vortexes number during the melting process. The critical Rayleigh number based on the mean thickness of the liquid layer and characterizing the vortexes apparition is established at  $Ra_{crit} = 4,575$ . The numerical



Notes:  $N_\psi = 15$ ,  $\Psi_{min} = -4.10^{-7}$ ,  $\Psi_{max} = 4.10^{-7}$

**Figure 24.** Comparison between the present model and Wintruff model: streamlines for the aspect ratio 1:8 in the convective zone

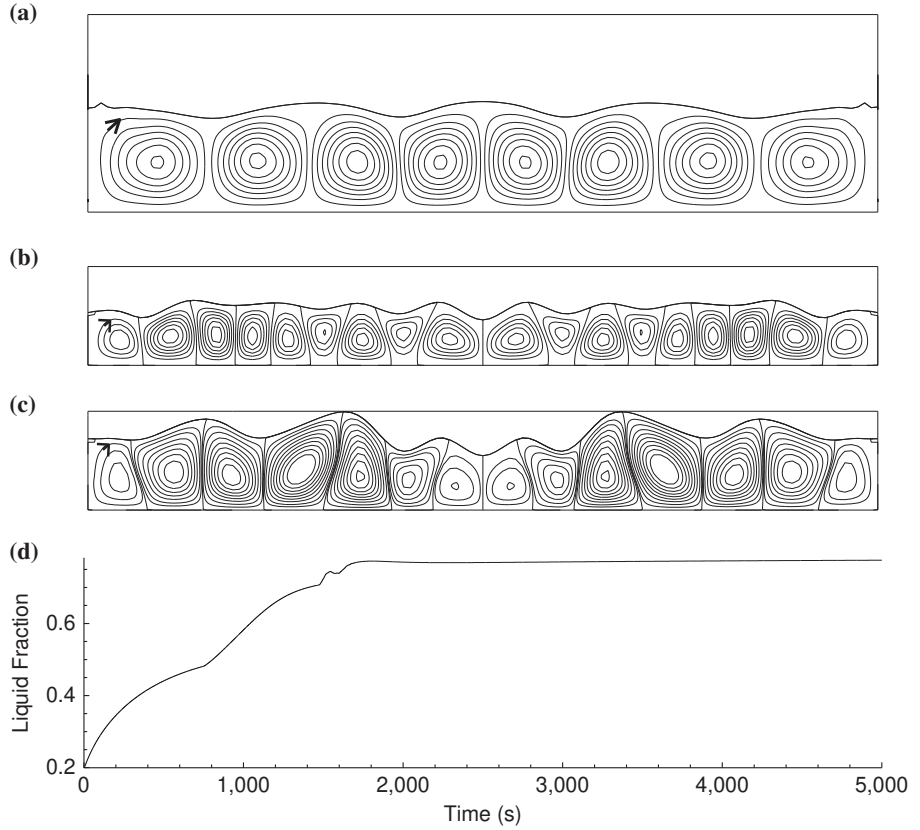


**Figure 25.** (a) Streamlines for the aspect ratio 1:4 in the convective zone; (b) and (c) streamlines for the aspect ratio 1:8 in the convective zone and the steady state regime, respectively; (d) liquid fraction evolution for the aspect ratio 1:8

**Notes:** (a)  $N_\psi = 20$ ,  $\Psi_{min} = -4.10^{-7}$ ,  $\Psi_{max} = 4.10^{-7}$ ; (b)  $N_\psi = 15$ ,  $\Psi_{min} = -4.10^{-7}$ ,  $\Psi_{max} = 4.10^{-7}$ ; (c)  $N_\psi = 19$ ,  $\Psi_{min} = -1.10^{-6}$ ,  $\Psi_{max} = 1.10^{-6}$

solutions was performed using spectral collocation methods whose main features were recalled. The study on numerical results accuracy shows that:

- All parameters, time-steps and polynomials developments orders are linked and must be chosen carefully to assume optimal accuracy results.
- The critical time  $t_{crit}$  representing the transition from conductive phase to convective region is independent of time-steps and polynomials developments orders parameters. This result is of great importance and confirms the high precision and the good stability of our numerical methods.

Compared to models based on classical methods such as finite differences, finite volumes, finite elements, etc., the present numerical method leads to the following remarks:

- The accuracy of the present model is high.
- The computational code is easier to build compared to the finite elements codes, for example.

- If we consider the CPU time, the present model needs few minutes to compute the numerical equations. This result traduces the efficiency of our model, easier and more adapted to solve this particular problem.

Nevertheless, compared to some industrial codes, our model has some disadvantages, such as:

- The time-dependent physical properties that induce non-linear coupled unsteady terms in Navier-Stokes and energy equations are not taken into account in the present model. In view to include this feature, the present model is actually extended to these coupled situations.
- This problem requires smoother geometries. One can try to palliate this disadvantage by constructing smoother approximations of non-smooth geometries.
- The augmentation of polynomials developments orders increases strongly the computing time.
- When the external heat flux or temperature imposed at the PCM is very greater than the temperature of the PCM melting, we must choose carefully some data to assume the algorithms convergence, for example some convergence conditions impose small time steps, and the CPU time on classical computers can make the present code prohibitive.

In a final analysis, this numerical method based on a suitable spectral method is of a good accuracy. One of its originality is the choice of Chebyshev polynomials basis in both axial and radial directions, and the good approximation of the interface solid/liquid. The automatic construction of these polynomials basis is of a great interest. These particular mathematical and numerical tools have permitted the resolution of this non-obvious problem.

In a second paper, we will study the effect of some boundary conditions, such as temperature or heat flux modulations, on the development of unsteady vortexes and its consequences on the charge and discharge processes in energy storage cells.

## References

- Badar, M.A. and Zubair, S.M. (1995), "On thermoeconomic sofa sensible heat, thermal energy storage systems", *J. Solar Energy Eng*, Vol. 117 No. 1, pp. 255-259.
- Batchi, M. (2005), "Etude Mathématique et Numérique des Phénomènes de Transferts Thermiques liés aux Ecoulements Instationnaires en Géométrie Axisymétrique", Thèse de Doctorat Mathématiques Appliquées, Université de Pau, Pau.
- Batina, J., Batchi, M., Blancher, S., Creff, R. and Amrouche, C. (2009), "Convective heat transfer augmentation through vortex shedding in sinusoidal constricted tube", *International Journal of Numerical Methods for Heat and Fluid Flow*, Vol. 19 Nos 3/4, pp. 374-395.
- Batina, J., Blancher, S., Amrouche, C., Batchi, M. and Creff, R. (2011), *Convective Heat Transfer of Unsteady Pulsed Flow in Sinusoidal Constricted Tube (ISBN 978-953-307-582-2)*, InTech, Amimul Ahsan, Rijeka, pp. 83-106.
- Bejan, A. (1996), "Entropy generation minimization: the new thermodynamics of finite-size devices and finite-time processes", *J. Applied Physics*, Vol. 79 No. 3, pp. 1191-1218.
- Bernardi, C. and Maday, Y. (1992), *Approximations spectrales de problèmes aux limites elliptiques*, Springer-Verlag, Berlin Heidelberg.

- Canuto, C., Hussaini, M.Y., Quarteroni, A. and Zang, T.A. (1988), *Spectral Methods in Fluids Dynamics*, Springer-Verlag, Berlin Heidelberg.
- Cao, Y. and Faghri, A. (1991), "Performance characteristics of a thermal energy storage module: a transient PCM/forced convection conjugate analysis", *International Journal of Heat and Mass Transfer*, Vol. 34 No. 7, pp. 93-101.
- Charach, C. and Conti, M. (1995), "Thermodynamics of latent heat storage in parallel or in series with a heat engine", *J. Appl. Phys*, Vol. 78 No. 3, pp. 1430-1437.
- Diaz, L.A. and Viscanta, R. (1984), "Visualization of the solid-liquid interface morphology formed by natural convection during melting of a solid from below", *International Communications in Heat and Mass Transfer*, Vol. 11 No. 1, pp. 35-43.
- Dietsche, C. and Müller, U. (1985), "Influence on Bénard convection on solid/liquid interfaces", *Journal of Fluid Mechanics*, Vol. 161, pp. 249-268.
- Fteiti, M. and Nasrallah, S.B. (2004), "Numerical study of interaction between the fluid structure and the moving interface during the melting from below in a rectangular closed enclosure", *Computational Mechanics*, Vol. 35 No. 3, pp. 161-169.
- Gau, C., Viskanta, R. and Ho, C.J. (1983), "Flow visualization during solid-liquid phase change heat transfer II. Melting in rectangular cavity", *Int. Comm. Heat Mass Transfer*, Vol. 10 No. 3, pp. 183-190.
- Gelfgat, A.Y. (2004), "Stability and slightly supercritical oscillatory regimes of natural convection in a 8:1 cavity: solution of the benchmark problem by a global Collocation method", *International Journal of Numerical Methods in Fluids*, Vol. 44 No. 2, pp. 135-146.
- Gong, Z. and Mujumdar, A. (1998), "Flow and heat transfer in convection-dominated melting in a rectangular cavity heated from below", *International Journal of Heat and Mass Transfer*, Vol. 41 No. 17, pp. 2573-2580.
- Guerrero, A.H., Aceves, S.M., Ruiz, C.E. and Cervantes, J.C.B. (1999), "Modelling of the charge and processes in discharge energy storage cells", *Energy Conversion & Management*, Vol. 40 Nos 15-16, pp. 1753-1763.
- Hale, N.W. and Viskanta, R. (1980), "Solid-liquid phase change heat transfer from above or below", *International Journal of Heat and Mass Transfer*, Vol. 23 No. 3, pp. 283-292.
- Jellouli, Y., Chouikh, R., Guizani, A. and Belghith, A. (2007), "Numerical study of the moving boundary problem during melting process in a rectangular cavity heated from below", *American Journal of Applied Sciences*, Vol. 4 No. 4, pp. 251-256.
- Kouksou, T., Arid, A., Majid, J. and Zeraouli, Y. (2010), "Numerical modeling of double-diffusive convection in ice slurry storage tank", *International Journal of Refrigeration*, Vol. 33 No. 8, pp. 1550-1558.
- Mithal, P. and Yang, K.T. (1994), "A phase change material based thermal energy storage option for house hold refrigerators", *ASME 94-WA/HT*, Vol. 5, pp. 1-8.
- Rubinstein, L. (1971), *The Stefan Problem. Translation of Mathematical Monographs*, Vol. 27, American Mathematical Society, Providence, RI.
- Seki, N., Fukosako, S. and Sugawara, M. (1977), "A criteria on onset of free convection in a horizontal melted water layer with free surface", *Transactions of ASME Series C, Journal of Heat Transfer*, Vol. 99 No. 1, pp. 92-98.
- Shen, J. (1994), "Efficient spectral-Collocation method I: direct solvers for the second and fourth order equations using Legendre polynomials", *SIAM J. Sci. Comput*, Vol. 15 No. 6, pp. 1489-1505.
- Shen, J. (1995), "Efficient spectral-Collocation methods II: direct solvers of second and fourth order equations by using Chebyshev polynomials", *SIAM J. Sci. Comput*, Vol. 16 No. 8, pp. 74-87.

- Shen, J. (1997), "Efficient spectral-Collocation methods III: polar and cylindrical geometries", *SIAM J. Sci. Comput.*, Vol. 18 No. 6, pp. 1583-1604.
- Wintruff, I., Günther, C. and Class, G. (2001), "An interface-tracking control-volume finite-element method for melting and solidification problems – part II: verification and application", *Numerical Heat Transfer, Part B*, Vol. 39 No. 2, pp. 127-149.
- Yen, Y.C. (1980), "Free convection heat transfer characteristics in a melt water layer", *Journal of Heat Transfer*, Vol. 103 No. 3, pp. 550-556.
- Yen, Y.C. and Galea, F. (1968), "Onset of convection in a layer of water formed by melting of ice from below", *Physics of Fluid*, Vol. 11 No. 6, pp. 1263-1269.

### Further reading

- André, P., Creff, R. and Crabol, R. (1981), "Etude des conditions particulières de fréquence favorisant les transferts thermiques en écoulements pulsés en canalisation cylindrique", *International Journal of Heat and Mass Transfer*, Vol. 24 No. 7, pp. 1211-1219.
- André, P., Creff, R. and Batina, J. (1987), "Study of thermal fluid for pulsed flow with compressible fluids", *Numerical Methods in Thermal Problems, Fifth International Conference, Montreal*, pp. 149-154.
- Batina, J. (1995), "Etude numérique des écoulements instationnaires pulsés en canalisation cylindrique", Thèse de Doctorat Physique, Université de Pau, Pau.
- Batina, J., Creff, R. and Batchi, M. (2004), "Etude thermique convective d'un écoulement interne en géométrie axisymétrique sinusoïdale", *Actes du congrès SFT*, Vol. 4 No. 1, pp. 987-992.
- Batina, J., Creff, R., André, P. and Blancher, S. (1989), "Numerical model for dynamic and thermal developments of a turbulent pulsed ducted flow", *Proceedings Eurotherm*, Vol. 1 No. 9, pp. 50-57.
- Batina, J., André, P., Creff, R. and Blancher, S. (1991), "Dynamic and thermal developments of a pulsed laminar compressible ducted flow", *Proceedings Eurotherm*, Vol. 1 No. 25, pp. 227-234.
- Blancher, S. (1991), "Transfert convectif stationnaire et stabilité hydrodynamique en géométrie périodique", Thèse de Doctorat Physique, Université de Pau, Pau.
- Cebeci, T. (1973), "A model for eddy conductivity and turbulent Prandtl number", *International Journal of Heat and Mass Transfer*, Vol. 95 No. 2, pp. 227-234.
- Chakravarty, S. and Sannigrahi, A.K. (1999), "A nonlinear mathematical model of blood flow in a constricted artery experiencing body acceleration", *Mathematical and Computer Modeling*, Vol. 29 No. 8, pp. 9-25.
- Charalampos, K. and Tsamopoulos, J. (2000), "Concentric core-annular flow in a circular tube of slowly varying cross-section", *Chemical Engineering Science*, Vol. 55 No. 22, pp. 5509-5530.
- Creff, R., Batina, J. and André, P. (1985), "A numerical model for a pulsed laminar flow with slightly compressible fluid", *Numerical Methods in Laminar and Turbulent Flow, Fourth International Conference, Swansea*, pp. 63-72.
- Fedele, F., Hitt, D.L. and Prabhu, R.D. (2005), "Revisiting the stability of pulsatile flow", *European Journal of Mechanics and Fluids*, Vol. 24 No. 2, pp. 237-254.
- Ghaddar, N.K., Magen, M., Mikic, B.B. and Patera, A. (1986), "Numerical investigation of incompressible flow in grooved channels, resonance and oscillatory heat transfer enhancement", *Journal of Fluid Mechanics*, Vol. 168, pp. 541-567.
- Guo-Tao, L., Xian-Ju, W., Bao-Quan, A. and Liang-Gang, L. (2004), "Numerical study of pulsating flow through a tapered artery with stenosis", *Chinese Journal of Physics*, Vol. 42 Nos 4-I, pp. 401-406.

- Gurek, C., Guleren, K.M., Aydin, K. and Pinarbasi, A. (2002), "Steady laminar flow computation through vascular tube constrictions", *Proceedings of the 6th Biennial Conference on ESDA, Bio-010*, pp. 1-7.
- Hemida, H.N., Sabry, M.N., Abdel-Rahim, A. and Mansour, H. (2002), "Theoretical analysis of heat transfer in laminar pulsating flow", *International Journal of Heat and Mass Transfer*, Vol. 45, pp. 1767-1178.
- Lee, B.S., Kang, L.S. and Lim, H.C. (1999), "Chaotic mixing and mass transfer enhancement by pulsatile laminar flow in an axisymmetric wavy channel", *International Journal of Heat and Mass Transfer*, Vol. 42, pp. 2571-2581.
- Moschandreau, T. and Zamir, M. (1997), "Heat transfer in a tube with pulsating flow and constant heat flux", *International Journal of Heat and Mass Transfer*, Vol. 40 No. 10, pp. 2461-2466.
- Ryval, J., Straatman, A.G. and Steinman, D.A. (2003), "Low Reynolds number modeling of pulsatile flow in a moderately constricted geometry", *Proceedings of the 11th Annual Conference of the CFD Society of Canada*, Vol. 1, pp. 300-304.
- Sobey, I.J. (1980), "On flow through channels. Part 1: calculated flow patterns", *Journal of Fluid Mechanics*, Vol. 96 No. 1, pp. 1-26.
- Uchida, S. (1956), "The pulsating viscous flow superposed on the steady laminar motion of incompressible fluid in a circular duct", *Z. Angew. Math. Phys.*, Vol. 7, pp. 403-422.
- Young Kim, S., Ha Kang, B. and Min Hyun, J. (1998), "Forced convection heat transfer from two heated blocks in pulsating channel flow", *International Journal of Heat and Mass Transfer*, Vol. 41 No. 3, pp. 625-634.
- Zhixiong, G. and Hyung Jin, S. (1997), "Analysis of the Nusselt number in pulsating pipe flow", *International Journal of Heat and Mass Transfer*, Vol. 40 No. 10, pp. 2486-2489.